

## HIGH-ANGULAR-RESOLUTION AND HIGH-SENSITIVITY SCIENCE ENABLED BY BEAMFORMED ALMA

VINCENT FISH<sup>1</sup>, WALTER ALEF, JAMES ANDERSON, KEIICHI ASADA<sup>1</sup>, ALAIN BAUDRY, AVERY BRODERICK<sup>1</sup>, CHRIS CARILLI<sup>1</sup>, FRANCISCO COLOMER, JOHN CONWAY<sup>1</sup>, JASON DEXTER, SHEPERD DOELEMEN<sup>1</sup>, RALPH EATOUGH, HEINO FALCKE<sup>1</sup>, SÁNDOR FREY, KRISZTINA GABÁNYI, ROBERTO GÁLVAN-MADRID, CHARLES GAMMIE, MARCELLO GIROLETTI, CIRIACO GODDI, JOSE L. GÓMEZ, KAZUHIRO HADA, MICHAEL HECHT, MAREKI HONMA<sup>1</sup>, ELIZABETH HUMPHREYS, VIOLETTE IMPELLIZZERI, TIM JOHANNSEN, SVETLANA JORSTAD, MOTOKI KINO, ELMAR KÖRDING, MICHAEL KRAMER, THOMAS KRICHBAUM<sup>1</sup>, NADIA KUDRYAVTSEVA, ROBERT LAING<sup>1</sup>, JOSEPH LAZIO, ABRAHAM LOEB, RU-SEN LU, THOMAS MACCARONE, ALAN MARSCHER<sup>1</sup>, IVÁN MARTÍ-VIDAL, CARLOS MARTINS, LYNN MATTHEWS, KARL MENTEN, JON MILLER, JAMES MILLER-JONES, FÉLIX MIRABEL, SEBASTIEN MULLER, HIROSHI NAGAI, NEIL NAGAR<sup>1</sup>, MASANORI NAKAMURA, ZSOLT PARAGI, NICOLAS PRADEL, DIMITRIOS PSALTIS<sup>1</sup>, SCOTT RANSOM, LUIS RODRÍGUEZ, HELGE ROTTMANN, ANTHONY RUSHTON, ZHI-QIANG SHEN<sup>1</sup>, DAVID SMITH, BENJAMIN STAPPERS, ROHTA TAKAHASHI<sup>1</sup>, ANDREA TARCHI, REMO TILANUS, JORIS VERBIEST, WOUTER VLEMMINGS, R. CRAIG WALKER, JOHN WARDLE, KAI WIJK, ÉRIK ZACKRISSON, & J. ANTON ZENSUS

### ABSTRACT

An international consortium is presently constructing a beamformer for the Atacama Large Millimeter/submillimeter Array (ALMA) in Chile that will be available as a facility instrument. The beamformer will aggregate the entire collecting area of the array into a single, very large aperture. The extraordinary sensitivity of phased ALMA, combined with the extremely fine angular resolution available on baselines to the Northern Hemisphere, will enable transformational new very long baseline interferometry (VLBI) observations in Bands 6 and 7 (1.3 and 0.8 mm) and provide substantial improvements to existing VLBI arrays in Bands 1 and 3 (7 and 3 mm). The ALMA beamformer will have impact on a variety of scientific topics, including accretion and outflow processes around black holes in active galactic nuclei (AGN), tests of general relativity near black holes, jet launch and collimation from AGN and microquasars, pulsar and magnetar emission processes, the chemical history of the universe and the evolution of fundamental constants across cosmic time, maser science, and astrometry.

#### 1. PREAMBLE

The science case for the ALMA beamformer reflects the broad scientific goals of the VLBI community. Astronomers were solicited for input at a variety of meetings including the 10th European VLBI Network (EVN) Symposium (Manchester 2010), the XXX URSI General Assembly (Istanbul 2011), Bringing Black Holes Into Focus: The Event Horizon Telescope (Tucson 2012), Outflows, Winds and Jets: From Young Stars to Supermassive Black Holes (Charlottesville 2012), From Stars to Black Holes: mm-VLBI with ALMA and Other Telescopes (Garching 2012), and the 11th EVN Symposium (Bordeaux 2012). This document includes input from scientists in all ALMA regions and is designed to be a living document, envisaged to evolve as new science areas are developed and existing areas refined by the community.

The case for science with beamformed ALMA is broad, ranging from Galactic to extragalactic science and touching on questions of vital importance for fundamental physics.

- ALMA VLBI observations of nearby supermassive black holes in Bands 6 and 7 will produce the first Schwarzschild-radius-scale images of nuclear black hole accretion disks and jets. With this resolution, astronomers will be able to perform new tests of general relativity and the no-hair theorem in a strong-field environment and understand in detail how magnetized plasmas are accreted and launched into relativistic jets that extend out to kiloparsec scales (Section 3).
- High-resolution imaging of AGN jets in conjunction with VLBI arrays in Bands 3 and 1 will clarify the internal jet structure, the role of magnetic fields in jet launch and collimation, and connections with very-high-energy (VHE) photon emission (Section 4).

- Observations of pulsars at millimeter wavelengths will shed light on the processes that produce coherent centimeter-wavelength emission, and searches for pulsars toward the Galactic Center, which can be done commensally with other Galactic Center observations. The detection of a pulsar in orbit near Sgr A\* that could also be used to probe the Kerr metric around the black hole with high precision (Section 5).
- Spectral-line VLBI of absorbing systems will measure the chemical evolution of the universe over cosmic time and test whether the fundamental constants of nature are actually variable (Section 6).
- VLBI observations of masers will refine estimates of the physical conditions and dynamics in the circumstellar gas around young stellar objects as well as in the circumnuclear environment of AGN (Section 7).
- Astrometry will clarify the structure of the Milky Way and obtain geometric distances to Galactic and extragalactic objects (Section 8).

In order to address these scientific topics, phased ALMA will primarily be used as a crucial station in millimeter and submillimeter VLBI arrays. However, it will also be valuable as a stand-alone instrument (e.g., for high-frequency pulsar observations).

#### 2. ENHANCED VLBI CAPABILITIES PROVIDED BY THE ALMA BEAMFORMER SYSTEM

The ALMA beamformer will most frequently be used in conjunction with other VLBI telescopes. ALMA's most significant contributions to VLBI arrays will be superlative sensitivity and higher angular resolution. The aggregated collecting area of 50 ALMA 12-m telescopes is equivalent to that of a single telescope with a diameter of  $\sim 84$  m. This large

TABLE 1  
EXPECTED NOISE CHARACTERISTICS OF PHASED ALMA

Band Number	Frequency (GHz)	Weather (octile)	$T_{\text{sys}}$ (K)	Aperture Efficiency	SEFD (Jy)
3	95	4th	70	0.71	48
6	230	4th	97	0.68	70
7	340	4th	180	0.63	140
9	675	2nd	1150	0.43	1310
9	675	1st	850	0.43	970

NOTE. — System temperatures are taken from the ALMA Sensitivity Calculator. Aperture efficiencies are from Table 8.3 of the ALMA Technical Handbook (2012-06-04). Phasing losses have not been included. Median weather conditions are assumed at 340 GHz and below since VLBI scheduling will be constrained by conditions at other sites.

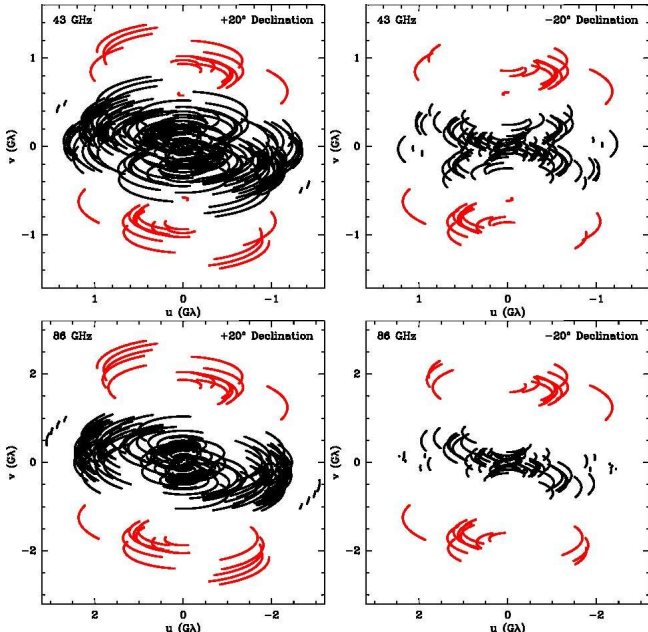


FIG. 1.— The  $(u, v)$  coverage of sources at  $+20^\circ$  (left) and  $-20^\circ$  (right) declination. The top row shows the global VLBI baseline coverage at 7 mm, and the bottom row shows the coverage at 3 mm. Baselines to ALMA are indicated in red. ALMA provides substantial improvement in the north-south coverage of global VLBI arrays, especially at 3 mm and for southern sources.

aperture, combined with excellent typical atmospheric conditions and low receiver noise temperatures, means that phased ALMA will be the most sensitive element in VLBI arrays.

The expected noise characteristics of ALMA in Bands 3, 6, 7, and 9 are summarized in Table 1. In Band 3 the system equivalent flux density (SEFD) of ALMA will be a factor of two better than the Green Bank Telescope (GBT) and nearly two orders of magnitude better than telescopes in the Very Long Baseline Array (VLBA). Band 3 continuum observations between ALMA and the GBT can provide a single-polarization rms noise of less than  $20 \mu\text{Jy}$  in 1 hr in a bandwidth of 4 GHz. Spectral line observations (as, for instance, of 86 GHz SiO masers) will achieve an rms of nearly 2 mJy in a  $1 \text{ km s}^{-1}$  velocity channel. At observing frequencies of 230 and 345 GHz, phased ALMA will improve upon the sensitivity of the phased SMA by more than a factor of 7 in rms noise on corresponding baselines.

ALMA will form very long baselines to existing VLBI stations, improving angular resolution. ALMA will more than double the north-south resolution of present 3 and 7 mm VLBI arrays (Figure 1). At higher frequencies, the fringe spacings of the longest baselines to ALMA are smaller than  $20 \mu\text{as}$ . Importantly, ALMA will provide not only increased angular

resolution but also  $(u, v)$  coverage that is critical for imaging at 230 GHz and above.

### 3. BLACK HOLES ON EVENT HORIZON SCALES

As the most extreme self-gravitating objects predicted by Einstein’s General Theory of Relativity (GR), black holes lie squarely at the intersection of astronomy and physics. They are now believed to reside at the heart of the vast majority of galaxies, and power a subset of X-ray binaries. Black holes play a critical role at the endpoints of stellar evolution, as the engines of gamma-ray bursts (the brightest events in the universe), in the formation and evolution of galaxies via feedback, and in powering the high-energy phenomena associated with active galactic nuclei (e.g., launching relativistic jets and producing the extraordinary electromagnetic luminosities observed.)

Resolving the immediate environment of a black hole on scales of the event horizon promises to provide sorely needed empirical insight into the impact of the black hole upon all of these processes. It is in this near-horizon environment where the accretion luminosity and relativistic outflows are produced, with potential implications on galactic and intergalactic scales. Realization of this goal requires angular resolution that only (sub)millimeter VLBI can provide (Falcke et al. 2000). The black hole with the largest apparent angular size, Sgr A\*, subtends tens of *microarcseconds*. However, successful observations using the technique of 1.3 mm VLBI have made it clear that imaging the emission at the event horizon is now within reach.

The most compelling evidence for this exciting possibility is the detection of structure on scales of  $4 r_{\text{Sch}}$  (Schwarzschild radius) in Sgr A\*, the  $\sim 4$  million  $M_\odot$  black hole at the center of our galaxy (Doeleman et al. 2008). These results were obtained using a 3-station 1.3 mm VLBI array, and continued observations with an enhanced 1.3 mm VLBI network have now measured time variability on  $r_{\text{Sch}}$  scales in Sgr A\* (Fish et al. 2011) and revealed structure at the very base of the relativistic jet in M87 (Doeleman et al. 2012). These results confirm the power of (sub)millimeter VLBI to resolve regions at the black hole boundary where strong gravity is dominant, creating an opportunity of immense scientific potential.

Existing 1.3 mm and 0.8 mm telescopes have in recent years engaged in an effort to produce a network of telescopes to be used for millimeter and submillimeter VLBI. Transforming this array into a wide-bandwidth, short-wavelength VLBI network that spans the globe, will achieve the resolution, sensitivity, and baseline coverage required to make true images of the event horizon. A critical step will be the inclusion of ALMA as a phased and beamformed single element in this observing array, the technical project described in this document. Parallel efforts to wide-band VLBI instrumentation to match ALMA bandwidths are funded and underway at other potential network sites.

This combination of phasing ALMA and increased bandwidth will advance three important areas that will dramatically enhance the current 1.3 mm VLBI array and enable future 0.8 mm VLBI.

**Sensitivity:** Recording up to 8 GHz of bandwidth and coherently phasing ALMA will lead to more than an order of magnitude sensitivity increase over current 1.3 mm VLBI arrays. One of the greatest impacts of this extraordinary leap in sensitivity will be the reliable measurement of interferometric phase, leading to first imaging capability.

**Polarization:** Focused efforts to enable dual-polarization recording at 1.3 mm and 0.8 mm VLBI telescopes will

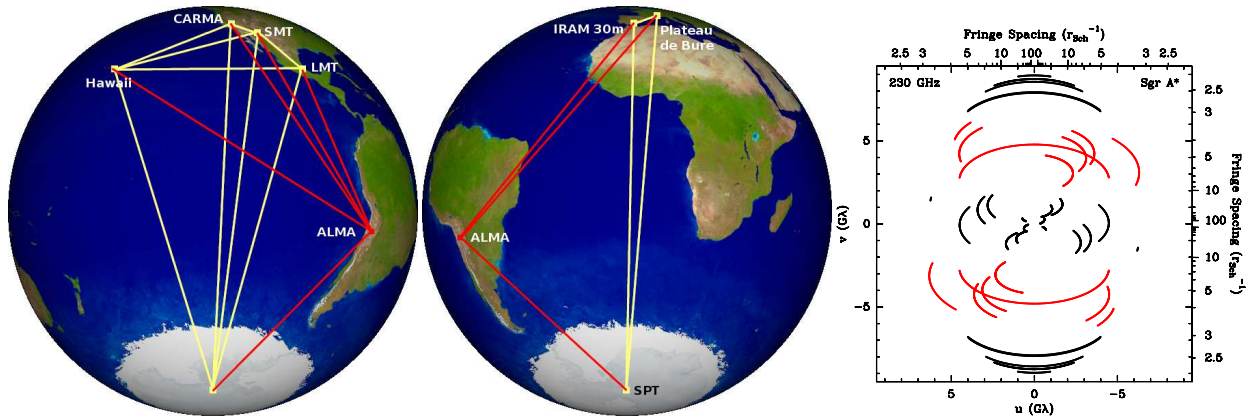


FIG. 2.— Left and middle: The potential 1.3 mm VLBI network as viewed from the declination of Sgr A\*. Right: The corresponding  $(u, v)$  coverage, with fringe spacings marked in units of  $r_{\text{Sch}}$ . Baselines to ALMA are marked in red in all panels.

allow full-polarization VLBI data sets (all four Stokes parameters). This capability will lead to new areas of research that target magnetic field structure near the event horizon.

**Baseline Coverage:** Addition of new 1.3 mm and 0.8 mm VLBI sites over the next three years will increase imaging fidelity, sensitivity, and temporal coverage of both Sgr A\* and M87. The scheduled addition of ALMA (2015), and inclusion of the South Pole Telescope (now a fully-funded project) and the proposed Greenland Telescope will provide important new high resolution baselines that enable imaging and sensitive tests for time variable  $r_{\text{Sch}}$ -scale structures (Figure 2).

These new capabilities have the potential to fundamentally transform our understanding of black holes on event horizon scales. Due to their mass and proximity, the two prime targets for such high-resolution studies are the black holes in the centers of the Milky Way (Sagittarius A\*) and Virgo A (M87). At a distance hundreds of times smaller than that to the next nearest supermassive black hole (SMBH), Sgr A\* can be studied in unparalleled detail and therefore plays an important role in astrophysics. On scales much larger than those probed by VLBI, the world’s most powerful optical/IR telescopes have been trained on Sgr A\* for years to directly observe the orbits of stars around the black hole and thereby measure its mass and distance (Ghez et al. 2008; Gillessen et al. 2009a). From these and other observations, the case for linking Sgr A\* with a  $\sim 4 \times 10^6 M_{\odot}$  SMBH is extremely strong (Reid 2009a and references therein). Among the most compelling pieces of evidence is the new intrinsic size of Sgr A\* measured using 1.3 mm VLBI, which implies a central mass density in excess of  $9.3 \times 10^{22} M_{\odot} \text{pc}^{-3}$ , ruling out all but the most exotic black hole alternatives (Maoz 1998). At a distance of 8 kpc, the Schwarzschild radius of this black hole subtends  $r_{\text{Sch}} \approx 10 \mu\text{as}$  (corresponding to an *apparent horizon diameter* of  $\sim 50 \mu\text{as}$ ), making the apparent size of its event horizon the largest that we know of. VLBI at 1.3 mm wavelength can “see through” the interstellar medium that scatter broadens this source with a  $\lambda^2$  dependence. Unlike Sgr A\*, the giant elliptical galaxy M87 exhibits a relativistic jet from sub-parsec to kiloparsec scales and is possibly the best candidate for the study of jet formation and collimation on small scales with VLBI (Kovalev et al. 2007; Ly et al. 2007; Hada et al. 2011, 2013). At a distance of 16.7 Mpc, the  $\sim 6.4 \times 10^9 M_{\odot}$  central black hole (Gebhardt et al. 2011) has  $r_{\text{Sch}} \approx 7.5 \mu\text{as}$ , only slightly smaller than that of Sgr A\*.

### 3.1. Constraining the Spin and Viewing Angle of Sgr A\*

Sgr A\* is highly underluminous, with a bolometric luminosity of around  $10^{-8}$  times the Eddington limit. The emission from Sgr A\* is conventionally modelled as arising from a radiatively inefficient accretion flow (RIAF) in which the electron and ion temperatures are decoupled from one another (Narayan et al. 1995). The cool electrons are incapable of radiating much heat, while the hotter ions disappear through the event horizon or drive outflows (Yuan et al. 2003). Contributions from a jet component are also possible (Falcke et al. 1993).

Some physical constraints on RIAF models arise from fitting the multiwavelength properties of Sgr A\*, including the spectral energy density and the implied accretion rate from Faraday rotation and depolarization at millimeter wavelengths. However, spatially-resolved observations are necessary for unambiguously determining properties such as the spin of the black hole and the viewing geometry—indeed, for validating the RIAF model in general. VLBI data at 1.3 mm (Doeleman et al. 2008; Fish et al. 2011), which provide this much-needed resolution, have successfully been used to constrain these parameters, establishing that the spin vector of the black hole has a large inclination to the line of sight and identifying a clearly preferred orientation in the plane of the sky (Broderick et al. 2009, 2011a). More sophisticated general relativistic magnetohydrodynamic models of the emission (Mościbrodzka et al. 2009; Dexter et al. 2010) and even jet models (Markoff et al. 2007) reach consistent constraints, suggesting that the observed emission morphology is dominated by the geometry of the flow and the general relativistic beaming and lensing effects near the black hole rather than by turbulent microphysics in the accretion flow.

While the present three-station VLBI array has been very successful in determining the structure of Sgr A\*, some parameter degeneracies persist, largely because the marginal signal-to-noise ratio (S/N) of the VLBI data prevents use of VLBI phase information. The highly sensitive, very long baselines to phased ALMA will enable precise measurement of the closure phase, the sum of interferometric phase around a closed triangle of baselines. Inclusion of closure phase decisively removes symmetry-flip degeneracies that persist when using only VLBI amplitudes (Broderick et al. 2011b). Simulations (Figure 3) show that measurement of closure phase on triangles including ALMA will produce exceptionally tight constraints on the spin vector of the Sgr A\* black hole within the context of RIAF models.

### 3.2. Time-Domain Studies

One of the most promising areas where VLBI can make new contributions to the study of black hole physics is in

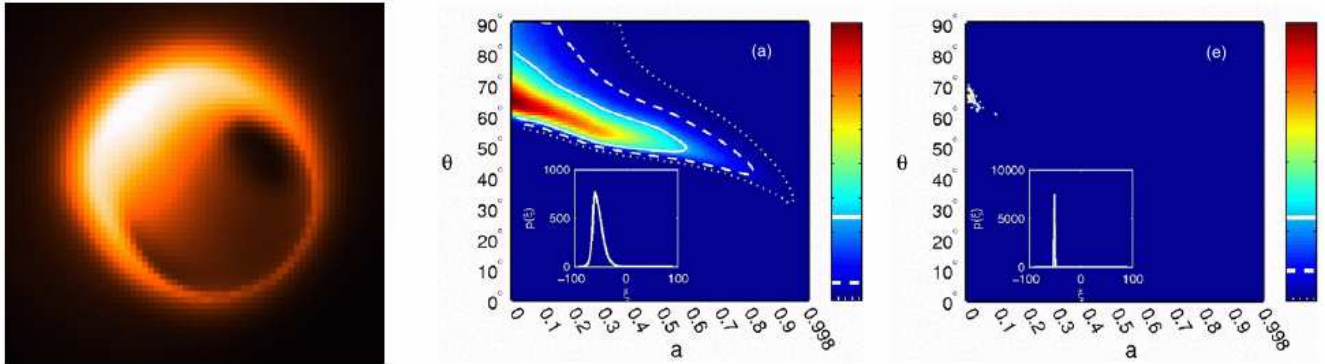


FIG. 3.— Left: The most likely RIAF model of the accretion flow in Sgr A\* (Broderick et al. 2011a). Middle: Probability contours for models parameterized by spin magnitude (abscissa) and inclination (ordinate) are shown in color, with the marginalized probability for the position angle in the plane of the sky indicated in the inset (Broderick et al. 2011b). Right: The probability contours tighten up dramatically when predicted closure phases from phased ALMA are included, and all three components of the black hole spin vector can be determined with great precision.

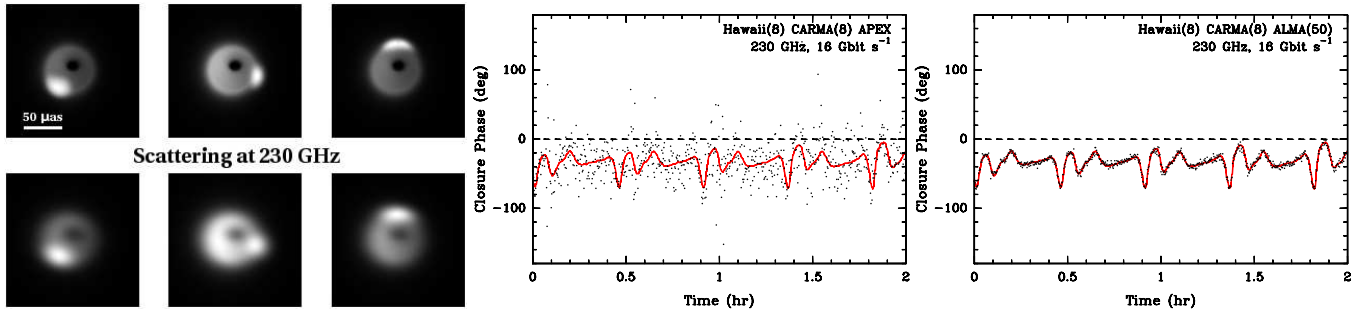


FIG. 4.— Signature of a hot spot orbiting a black hole at a radius of  $3 r_{\text{Sch}}$  with a period of 27 minutes. The model is shown at three equally-spaced orbital phases, with and without interstellar scattering. The plots show the expected closure phases on a triangle of stations including the phased SMA, phased CARMA, and either a single telescope in Chile (e.g., APEX, middle) or phased ALMA (right). The red curve shows the expected closure phase signal in the absence of noise, and the black points show simulated data at a time cadence of 10 s (comparable to the coherence time of the atmosphere). The substantial sensitivity improvement provided by phased ALMA will allow rapid time-domain studies of the variable accretion flow in Sgr A\*. (Figure adapted from Doeleman et al. 2009)

searching for time-variable structures due to inhomogeneities in the accretion flow surrounding Sgr A\*. Localized heating in the inner accretion flow is a natural consequence of magnetic turbulence (Broderick & Loeb 2006; Dexter et al. 2010) and can give rise to orbiting “hot spots”, which have been used to explain the pronounced X-ray, near infrared and submillimeter flares in Sgr A\* (Yusef-Zadeh et al. 2006; Eckart et al. 2006; Marrone et al. 2008). VLBI cannot image these time-variable structures since they would be smeared out over a single observing epoch—for Sgr A\*, the innermost stable circular orbit (ISCO) has a period of 30 min for a non-spinning black hole ( $a = 0$ ), and only 4 min for one that has maximum spin ( $a = 1$ ). However, clear signatures of hot spots should be detectable by using closure phase. (For the more massive black hole in M87, the ISCO period is longer than an observing night, with the result that standard Earth-rotation aperture-synthesis imaging can be used to make movies during periods when the emission is variable.)

Simulations of such hot-spots that include full GR ray-tracing and radiative transfer (Doeleman et al. 2009; Fish et al. 2009b) show that baselines to ALMA can not only detect such hot spots using closure phase, but will have sufficient sensitivity to detect periodicity if the hot spots persist for multiple orbits in the accretion flow. Detection of periodicity would result in a new way to measure black hole spin and test the validity of the Kerr metric by studying ensembles of hot-spot orbits over many observing epochs.

Increased bandwidths combined with dual polarization receivers will also allow high sensitivity VLBI polarimetry of Sgr A\*. At 230 and 345 GHz, the measured low angular resolution linear polarization fraction of Sgr A\* is  $\sim 10\%$  (Aitken et al. 2000; Bower et al. 2003; Marrone et al. 2006,

2007), but models of magnetized accretion flows predict polarization fractions in excess of 30% and up to 60% on angular scales probed by 230 GHz VLBI (Bromley et al. 2001; Broderick & Loeb 2006). It is probable that all previous polarimetry of Sgr A\* has suffered from significant beam depolarization. Only (sub)millimeter VLBI polarimetry, particularly at the 345 GHz where source opacity is lowest and the blurring of interstellar scattering is least important, can observe the small-scale polarized structures that models predict, providing a very powerful new diagnostic of hot spots and accretion emission. On sensitive single VLBI baselines, weaker cross-polarized detections (e.g., between the right and left circular polarizations, RCP-LCP) can be phase-referenced to the stronger parallel detections (e.g., RCP-RCP), allowing searches for time-variable polarized emission on  $r_{\text{Sch}}$  scales.

### 3.3. Testing General Relativity with (Sub)Millimeter VLBI

Strong lensing due to general relativity around a black hole is predicted to produce detectable observational signatures. When a black hole is surrounded by an optically thin plasma, lensing should produce a bright photon ring with a dim “shadow” in its interior (Falcke et al. 2000). The shape of this shadow very closely approximates a circle for values of the spin  $a \lesssim 0.9$  (Takahashi 2004; Johannsen & Psaltis 2010b). Confirmation of this prediction would probe more deeply and cleanly into a relativistic potential than has ever been done before.

General relativity predicts not only the existence of the black hole shadow but also its size, which is proportional to the mass of the black hole. Some uncertainties remain regarding the mass of the black hole in Sgr A\* and its distance from the Earth (e.g., Ghez et al. 2008; Gillessen et al. 2009a,

2009b), although the predicted diameter of the shadow is approximately  $50 \mu\text{as}$ . A wide variety of models of the 1.3 mm emission, including models in which this emission arises in an accretion disk and others in which it originates from a jet, predict that the morphology of the emission will be dominated by general relativistic lensing, resulting in crescent-like images and a shadow that will be detectable on VLBI baselines to ALMA (e.g., Dexter et al. 2010). Similar results may be found for M87, although there is less agreement on the predicted morphology of the emitting region (e.g., Dexter et al. 2012). Conversely, if general relativity is assumed to be true, measuring the size of a black hole shadow provides an independent measurement of the ratio of the black hole mass to the source distance (Johannsen et al. 2012; Ruprecht 2012).

The shape of the photon ring also provides a test of the “no-hair” theorem, which states that the exterior spacetime of a black hole can be completely characterized by the black hole’s mass, spin, and electric charge. Since it is difficult to envision how a black hole could sustain a gravitationally relevant net electric charge (see Blandford & Znajek 1977), the only independent multipole moments of the spacetime of a real astrophysical black hole are the monopole and dipole moments, which correspond to the black hole mass and spin, respectively. In general relativity, all higher moments are expressible in terms of the mass and spin alone. The simplest theoretical spacetimes that violate this theorem assume a quadrupole moment  $Q = -M(a^2 + \epsilon M^2)$ , where  $a$  is the black hole spin,  $M$  is the mass, and  $\epsilon$  parameterizes the deviation from general relativity (Glampedakis & Babak 2006; Johannsen & Psaltis 2010a). When a nonzero quadrupole deviation is introduced, the shape of the photon ring and shadow becomes noncircular (Johannsen & Psaltis 2010b), imprinting a signature onto VLBI quantities that would be detectable with an observing array that includes phased ALMA (Figure 5). Similarly, many other alternative theories of gravitation make testable predictions for the properties of black hole shadows (e.g., the review by Falcke & Markoff 2013).

### 3.4. Observing Jet Launching on Schwarzschild Radius Scales

Jets are believed to be powered through extraction of energy from accreting supermassive black holes. Feedback from these jets enriches and heats the intergalactic medium and plays a role in galaxy formation. Mechanisms have been proposed to explain how energy and angular momentum can be extracted from the accretion flow or the spin of the black hole (e.g., Blandford & Znajek 1977; Blandford & Payne 1982), and general relativistic magnetohydrodynamic simulations are beginning to be able to model the magnetized plasmas in the inner accretion and outflow region (e.g., McKinney et al. 2012), but the lack of observations probing these small angular scales make it difficult to distinguish among classes of models that have the same behavior on large scales.

Recent observations have detected M87 on baselines between Hawaii and the western US, establishing that at 1.3 mm the inner jet is approximately  $38 \mu\text{as}$  ( $4.8 r_{\text{Sch}}$ ) in size (Figure 6 and Figure 7; Doeleman et al. 2012). This size favors models in which the jet is launched within a few Schwarzschild radii of the black hole (e.g., Nishikawa et al. 2005) rather than arising from magnetic fields anchored out past the ISCO of the disk (e.g., De Villiers & Hawley 2003). This size is also substantially smaller than the ISCO of a nonrotating black hole, which may suggest that the accretion flow rotates in a prograde sense around a spinning black hole. However, further observations on baselines oriented perpendicular to the roughly east-west direction of the Doeleman et al. (2012) detections, such as those between the US and

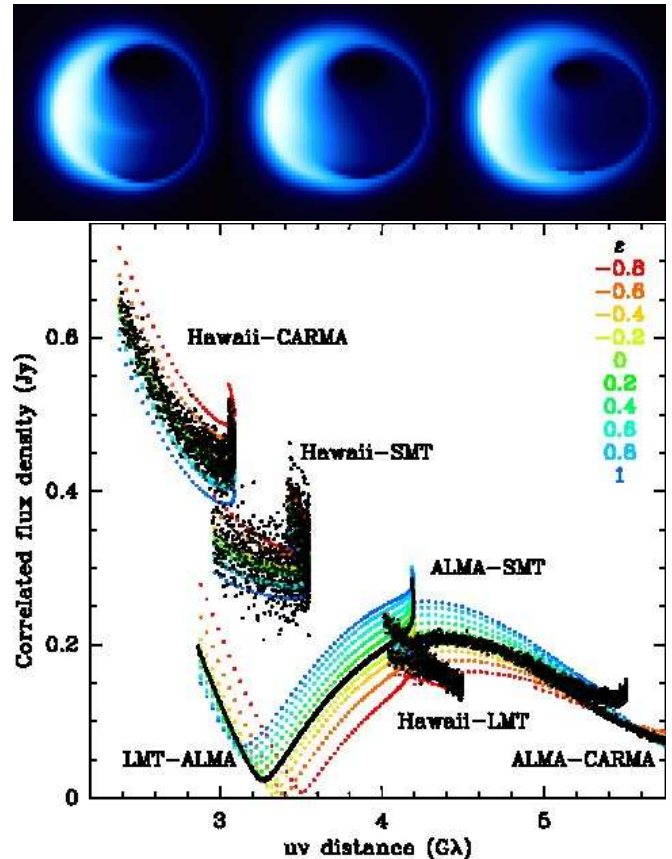


FIG. 5.— In spacetimes that do not obey the no-hair theorem near a black hole, the shadow can be noncircular. From left to right, the three top panels show model images (Broderick, A.E., Johannsen, T., Loeb, A., & Psaltis, D., in preparation) with  $\epsilon = -0.8$ ,  $\epsilon = 0$  (general relativity), and  $\epsilon = +1$ . These models predict measurably different amounts of correlated flux density on baselines between ALMA and North America (bottom, with simulated data overplotted).

ALMA, will be necessary to break degeneracies between this interpretation and other models.

At longer wavelengths, the inclusion of phased ALMA in VLBI imaging arrays can address questions relating to jet launch and collimation mechanisms. The jet in M87 has been observed to have a parabolic jet width profile on scales ranging from  $10^2$  to  $3 \times 10^5 r_{\text{Sch}}$  (Junor et al. 1999; Asada & Nakamura 2012). High-fidelity imaging at 3 mm is required to make the connection between the scales accessible to 1.3 mm VLBI (a few Schwarzschild radii) and the  $100 r_{\text{Sch}}$  scales observable at longer wavelengths. The structure of the M87 jet at 3 mm is observed to be highly variable, but Global mm-VLBI Array (GMVA) observations suffer from limitations in image fidelity and sensitivity. Higher-resolution jet images would allow a more precise measurement of the jet opening angle, which is predicted to be at least  $60^\circ$  if centrifugal acceleration along poloidal magnetic field lines connected to the accretion disk is responsible for jet formation (Blandford & Payne 1982). Polarimetric observations of the emission near the jet base would help clarify the three-dimensional geometry of the magnetic field that launches the jet. Multi-epoch observations at high fidelity will allow structures within the jet to be tracked, providing measurements of the velocity along the jet length. Motions in the jet are known to be superluminal at the location of the knot HST-1, approximately  $100 \text{ pc}$  ( $> 10^5 r_{\text{Sch}}$ ) from the black hole (Biretta et al. 1999; Cheung et al. 2007), but there is substantial observational disagreement as to whether the velocity at the jet base is highly subrelativistic, relativistic, or even superluminal (Kovalev et al. 2007; Ly et al. 2007; Acciari et al. 2009). The improved imaging ca-

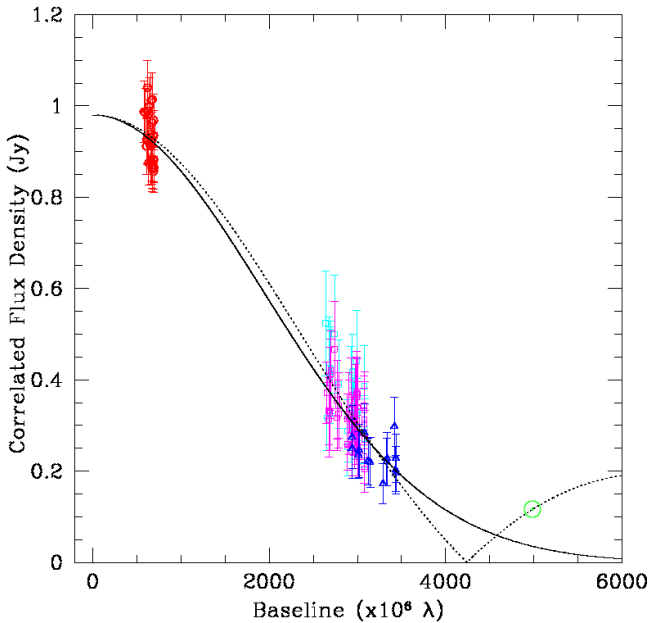


FIG. 6.— Detections of M87 with 1.3 mm VLBI observations in 2009 (Doeleman et al. 2012). The solid line shows a Gaussian fit to the data, approximating the emission from a forward jet, and the dotted line indicates a ring fit, approximating the expected emission from a lensed counterjet around the black hole shadow. The circled green point shows the  $1\sigma$  sensitivity on a simulated 10-s data point between phased ALMA and the SMT with an effective bandwidth of 4 GHz in two polarizations.

capability provided by the inclusion of phased ALMA in VLBI observing arrays will clarify the acceleration profile of the jet in M87.

### 3.5. Imaging Black Holes

Substantial scientific progress has been made to date understanding Sgr A\* and M87 with non-imaging techniques, but much of this work has necessarily been dependent on models of the assumed emission morphology based on physical intuition and unresolved multiwavelength observations. Direct imaging would provide a model-independent picture of the inner emitting region around supermassive black holes.

The prospects for imaging Sgr A\* or M87 in the next few years are great. Bispectral maximum entropy imaging methods originally developed for optical interferometry (e.g., BS MEM; Buscher 1994) have shown great promise in being able to produce image reconstructions from sparsely-sampled  $(u, v)$  coverage (e.g., Malbet et al. 2010). Monte Carlo imaging techniques, such as those used by the MACIM code (Ireland et al. 2006), also appear to be particularly well suited to millimeter VLBI (Ruprecht 2012). Compared to deconvolution-based methods, these forward-imaging algorithms are able to provide significantly better image quality and, in the case of sparse arrays, often succeed when CLEAN fails to converge at all.

An array consisting solely of phased ALMA and the three telescope sites in the US that have been participated in 1.3 mm VLBI observations (CARMA, SMT, Hawaii) can produce images that are sufficient to distinguish between models of the M87 jet that differ only on scales of a few  $r_{\text{Sch}}$ . Figure 8 shows two models, one of which has the jet forming close to the black hole with its emission strongly lensed into a “shadow” morphology. In the other model, the jet forms farther out from the black hole and the image is dominated by the approaching outflow, though a faint shadow is also observed. The addition of other antennas that are likely to be VLBI-capable at this wavelength before or shortly after the completion of the ALMA phasing project will enable much higher fidelity im-

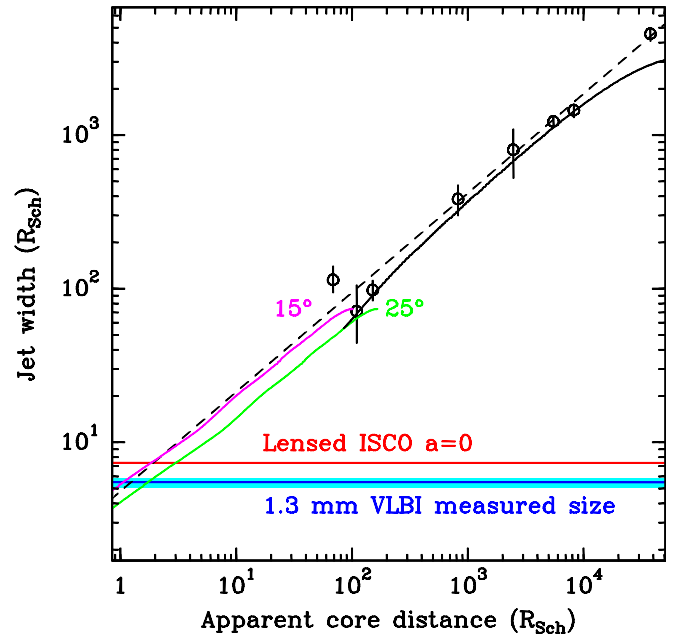


FIG. 7.— The measured size of the 230 GHz emission in M87 (blue, with the cyan region denoting the  $3\sigma$  error bars) is smaller than the lensed size of the innermost stable circular orbit for a nonrotating black hole (red). The size of the emission, which is known to originate from within a few Schwarzschild radii of the black hole (Hada et al. 2011), is consistent with both the observed  $r^{2/3}$  jet width profile seen at longer wavelengths (symbols, from Biretta et al. 2002) and the theoretical jet width profile (also  $r^{2/3}$ , shown in magenta and green for inclination angles of 15 and 25 degrees; courtesy J. McKinney). The figure is adapted from Doeleman et al. (2012).

ages to be produced. This is a possibility that can only be pursued with the sensitivity and baseline coverage provided by phased ALMA.

## 4. ACTIVE GALACTIC NUCLEI AND JET PHYSICS

Powered by accretion onto black holes with masses up to  $10^{10} M_{\odot}$ , AGNs represent the most energetic long-lived phenomenon in the universe. In  $\sim 10\%$  of these objects, a substantial fraction (as much as tens of percent) of the energy of accretion is converted into kinetic energy of outflows in the form of relativistic, highly collimated jets of energetic plasma and magnetic fields. The jets emit highly variable nonthermal radiation across the electromagnetic spectrum that can greatly exceed the thermal emission from the accretion disk and host galaxy in blazars, AGNs in which one of the jets points in our direction. In some cases, the bulk of the observed flux emerges in  $\gamma$ -ray photons in the GeV or even TeV energy range. One of the most intriguing and challenging quests of current astrophysics is to understand the physical conditions and processes that give rise to the formation of these relativistic jets, production of high-energy particles, and emission of  $\gamma$ -rays. Of particular interest is the question of how accretion onto SMBHs generates such high-powered directed outflows.

AGN jets have profound effects on the surrounding environment, e.g., in clusters of galaxies (McNamara et al. 2005). Energy and momentum exchange between jets and the intra-cluster medium between galaxies can regulate the formation and growth of galaxies and the SMBHs within them, as well as limit the rate of mergers and flows onto galaxies hosting SMBHs (Springel et al. 2005; Di Matteo et al. 2005). Moreover, radiation from the jets ionizes gas along a cone surrounding the channel of flow within the host galaxy. Shock waves form where jets ram into the external medium, inducing large bulk motion of gas and even triggering star formation. These effects are visible in AGNs today, but were even more prevalent at earlier epochs of the universe, when many galaxies were still in the formation phase and a greater proportion

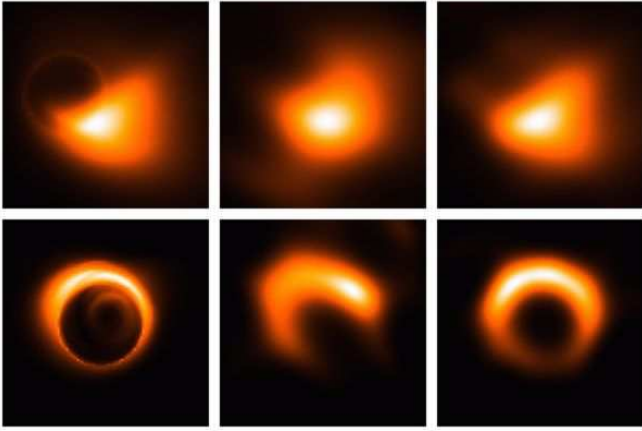


FIG. 8.— Models and simulated reconstructions of the innermost emitting region in M87. The top left image shows a model of a magnetically-dominated jet anchored in an accretion disk around the black hole with a footprint  $\sim 10 GM/c^2$  (Broderick & Loeb 2009). The bottom left image shows a model in which most of the jet emission arises within the photon sphere at 2 to 4  $GM/c^2$ , causing lensed counterjet emission to dominate in the observer’s frame (Dexter et al. 2012). Middle panels show BSMEM reconstructions of these models from simulated observations using an early array consisting only of phased ALMA, phased SMA, phased CARMA, and the SMT. Right panels show reconstructions from this array plus the IRAM 30-m telescope, the phased Plateau de Bure Interferometer, and the LMT. The early array can easily distinguish between the two classes of models. The full array can produce reasonable images of the emission, possibly providing a clear view of the shadow, from which the black hole mass can be measured directly.

were strongly active. Understanding galaxy formation and the birth of the early generations of stars is therefore intimately tied to our understanding of how black holes grow by accretion and generate relativistic jets, and how the jets propagate from the center of a galaxy to its outskirts and beyond.

#### 4.1. High-Resolution Jet Imaging

VLBI is the only technique currently capable of viewing directly the parsec- and subparsec-scale regions of jets in AGNs. At frequencies of 43 and 86 GHz, the jet is mostly optically thin. The VLBA currently provides angular resolution of  $\sim 100 \mu\text{as}$  in the east-west direction at wavelengths of 3 and 7 mm, but only  $\sim 250 \mu\text{as}$  in the north-south direction.

The inclusion of phased ALMA as a VLBI station will more than double the north-south resolution of 3 and 7 mm VLBI arrays (Figure 1). Such high-resolution observations can image the acceleration and collimation zone of the flow, which currently can be explored only in an indirect manner through time variability of flux and polarization. The jets of even the brightest blazars are challenging to detect with arrays composed of single-dish telescopes operating at 3 mm; adding phased ALMA would improve this dramatically.

The jets of radio-loud AGNs contain a bright, compact feature at the upstream end of 7 and 3 mm images. This is called the core, although in blazars and blazar-like radio galaxies there is considerable evidence that it lies more than 0.5 pc from the SMBH that powers the AGN (e.g., Chatterjee et al. 2009, 2011). The core is a key structure in a jet. At centimeter wavelengths what appears to be the core is generally just the transition between optically thick and thin emission, but at millimeter wavelengths it has the properties of a physical structure, such as a standing cone-shaped shock (Cawthorne 2006; D’Arcangelo et al. 2007; Marscher et al. 2008, 2010). Synchrotron models show that in some sources the 7 and 3 mm emission is optically thin enough to trace the recollimation shock (Figure 9).

A surprising result of recent studies that combine time sequences of 7 mm VLBA images with monitoring of flux across the electromagnetic spectrum is that, in many blazars,

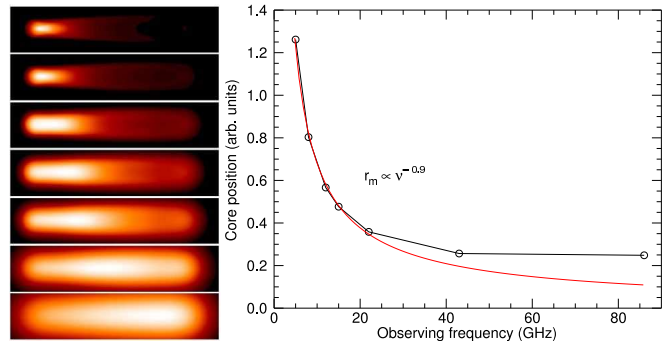


FIG. 9.— *Left, top to bottom*: Synchrotron models of a blazar jet at 86, 43, 22, 15, 12, 8, and 5 GHz (based on Gómez et al. 1995, 1997; Mimica et al. 2009). *Right*: The core location deviates from a Blandford & Königl (1979) jet model (red curve) at ALMA frequencies, indicative of the location of the recollimation shock.

most of the infrared, optical, X-ray, and  $\gamma$ -ray emission originates in or near the core. It is frustrating that the core is only slightly resolved (and not resolved at all in the north-south direction) at 7 mm. Currently, it is not generally resolved much better at 3 mm because the trans-continental baselines are too noisy. With the addition of ALMA, millimeter VLBI can resolve the cores in bright blazars as well as image a portion of the jet between the core and the central engine. By doing so, VLBI studies will address through direct imaging the key question of how ultra-relativistic jets are generated by accreting SMBHs. In particular, such imaging can provide clues regarding how and where the outflow transforms from purely electromagnetic to kinetic energy-dominated, and the relative roles played by velocity shear, turbulence, shocks, and plasma instabilities in the flow.

Some of the most exciting recent discoveries in AGN jets have arisen from studies of their structure transverse to the flow direction. Observations of large scale AGN jets with the VLA (Laing & Bridle 2002) show distinct velocity gradients in which a fast central spine is surrounded by a slower sheath that interacts with the external medium. It is not yet clear to what extent these interactions serve to stabilize and/or decelerate the flow, and how they influence the overall evolution and structure of the jet. Our knowledge is more limited on small scales, due to the need for high dynamic range polarimetric imaging, preferably with a symmetric beam. The addition of phased ALMA to VLBI arrays will provide significant improvement in these directions, allowing observations of limb brightening and changes in polarization that provide powerful probes of the flow properties.

#### 4.2. Connections to Optical Imaging

The European Space Agency’s Gaia optical astrometry mission (expected launch time late 2013) will provide astrometric and photometric observations of a large sample of QSOs down to  $V=20$  mag. Its astrometric accuracy will reach  $25 \mu\text{as}$ , and the observations of approximately a half million QSOs will eventually lead to the Gaia Celestial Reference Frame (GCRF). It will be possible to establish a direct connection between the radio-based International Celestial Reference Frame (ICRF2) and the optical-based GCRF for the first time (e.g. Charlot & Bourda 2012). Gaia is expected to provide information about the optical emission within 1 mas of the central engine—within a region of 8 pc of the SMBH at  $z \approx 1$  (e.g., Browne 2012, and references therein). A recent study (Popović et al. 2012) showed that Gaia will be able to detect variations in the inner structure of the QSOs via positional offsets of the optical photocenters. “Pre-Gaia” optical observations of QSOs by Antón et al. (2012) showed photocenter jittering of a few tens of parsecs in three sources ac-

accompanied by optical magnitude variations. These findings can be explained by either blobs or shocks traveling in the jet (very similar what is observed in the radio regime) or by double variable sources at the center of the objects—e.g., binary supermassive black holes (Popović et al. 2012). As of now, it is not clear whether the non-thermal optical and radio emission originate from the same location. With the inclusion of phased ALMA in millimeter VLBI, the radio emitting region can be measured and mapped even closer to the central engine, and thus the region where the optical emission measured by Gaia may originate can be mapped with high fidelity in the radio regime.

Gaia will observe  $\sim 500000$  QSOs. Using a conservative estimate for the proportion of compact, radio-loud, and millimeter-bright sources, a couple hundred sources will be observable with the millimeter VLBI array containing phased ALMA. This sample of radio sources thus can be studied by the highest resolution VLBI instrument in the millimeter regime, to investigate whether the observed optical characteristics can be connected to features in the jet launching region revealed in the millimeter regime.

#### 4.3. VHE Photon Production

An exciting discovery made by space-borne instruments and ground-based Cherenkov telescopes is the detection of VHE  $\gamma$ -rays from over 1000 AGN jets. There are currently several competing models for the source of this radiation, which include upscattering of synchrotron photons from either the jet (e.g., Bloom & Marscher 1996), accretion disk (Dermer & Schlickeiser 1994), broad emission-line region (Begelman et al. 1994), or dusty torus (Sikora et al. 2009) by relativistic electrons, and high-energy particle cascades (Mannheim et al. 1991). A feature common to all models, however, is that the  $\gamma$ -rays are associated with the compact regions of relativistic jets energized by the central SMBHs.

High angular resolution observations from millimeter VLBI, combined with  $\gamma$ -ray data from Fermi and ground-based Cherenkov telescopes, offer opportunities to significantly increase our understanding of VHE emission and particle acceleration mechanisms in AGN. The nearby radio galaxy M87 has exhibited several VHE flares in recent years, with inconsistent correlation between the radio and  $\gamma$ -ray photons (Hada et al. 2012, and references therein). One potential explanation is that variable magnetic field strengths near the black hole cause variable opacity at centimeter wavelengths, with the synchrotron self-absorption turnover frequency typically near 43 GHz. Multifrequency monitoring using VLBI with phased ALMA during a VHE flare would provide an observational test of this hypothesis (Figure 11).

In blazars, high energy photons may be produced near and upstream of the core. The Fermi Large Area Telescope (LAT) instrument is gathering well-sampled, continuous light curves of many bright  $\gamma$ -ray blazars. A collaboration led by A. Marscher (Boston U.) uses 7 and 3 mm VLBI to focus on a millimeter-bright subset (17) of these objects. So far, the results show that many  $\gamma$ -ray outbursts in these objects occur when a new superluminal knot passes through the core (Figure 10; Marscher et al. 2010; Jorstad et al. 2010; Agudo et al. 2011a,b). High-resolution imaging of this region is therefore vital for understanding the mechanisms by which these high-energy photons are produced (Blandford 2008).

#### 4.4. Double-Sided Radio Jets

Cygnus A, the closest ( $z = 0.057$ ) strong FR II radio galaxy, is a key object for detailed studies of its prominent double-sided jet and nucleus. Relativistic beaming effects are reduced due to the large inclination of the jet to the line of sight, al-

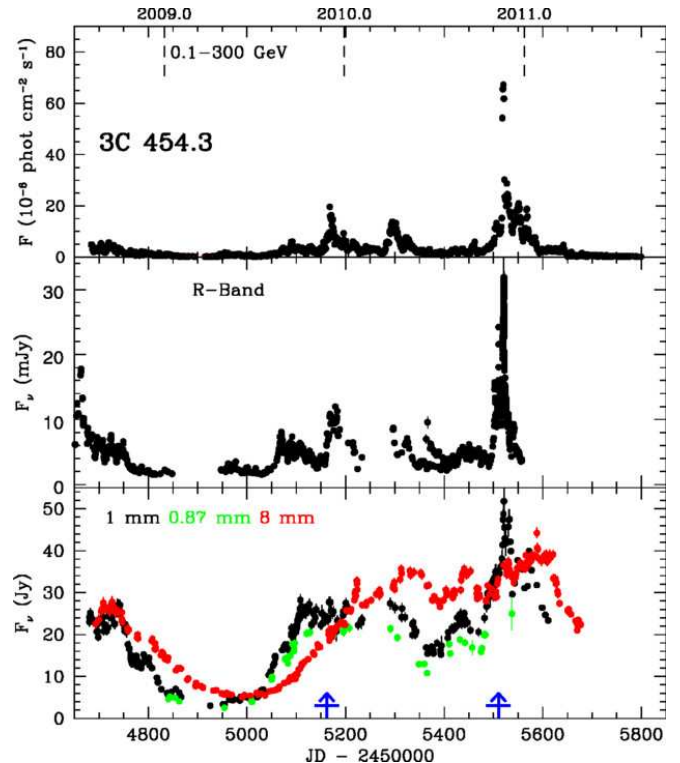


FIG. 10.— Multiwavelength light curves of the quasar 3C 454.3 during the extreme super outburst in late 2010. The general behavior across wavebands is similar, but the detailed light curves are quite different. The  $\gamma$ -ray light curve shows much greater correlation with the light curve at 1 mm than at 8 mm, suggesting that VLBI at submillimeter wavelengths may be better suited for probing the  $\gamma$ -ray emitting region. Vertical blue arrows in the bottom panel indicate times when a new superluminal knot passed through the core in 7 mm VLBA images. Data are from Jorstad et al. (in prep.) and Abdo et al. (2011).

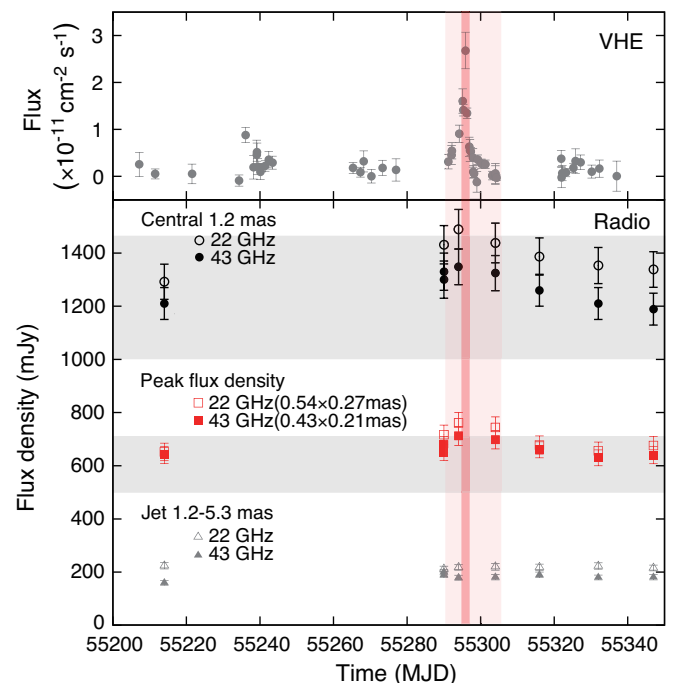


FIG. 11.— Centimeter light curves of the core of M87 correlate with the VHE  $\gamma$ -ray flare in 2010, suggesting that the VHE emission arises very near the black hole (Hada et al. 2012).



lowing geometrical effects to be disentangled from the internal jet speed. This makes Cyg A an ideal candidate to study jet physics in an object similar to those seen in more distant and luminous quasars (e.g., Barthel 1989).

The central engine and part of the innermost counterjet are likely obscured by free-free absorbing material in a thick torus (Carilli et al. 1994). The absorbing material should be optically thin in the (sub)millimeter regime. Important physical parameters of the obscuring torus (e.g., size, opacity, and temperature) can be determined from the jet-to-counterjet ratio, which is frequency-dependent. A kinematic study of the two-sided jet structure makes it possible to determine the jet speed and orientation in the circumnuclear region (Krichbaum et al. 1998; Bach et al. 2002). The accuracy of the determination of this ratio requires knowledge of the location of the true nucleus, located halfway between the footpoints of the jet and counterjet. This position can be determined more accurately at higher observing frequencies due both to the lower optical depth at high frequency and the higher angular resolution provided by the observing array. VLBI with ALMA in Bands 1 and 3 will allow determination of the core position to within a small fraction of the  $\sim 100 \mu\text{s}$  synthesized beamwidth.

Components of the main jet seem to accelerate from speeds of  $\beta \approx 0.1-0.2$  within 1 mas of the core (Krichbaum et al. 1998) to  $\beta \approx 0.3-0.7$  at 4 mas (Carilli et al. 1994; Bach et al. 2002; Krichbaum et al. 2008). VLBI observations at 7 mm reveal significant structural variability in the counterjet, with a lower velocity of  $\beta \approx 0.1-0.5$ . The relatively low apparent velocity in the counterjet could be due to an inherent asymmetry between the two sides of the jet. Jet stratification may be an alternate explanation, if different layers of the counterjet are being seen due to the viewing geometry. High-fidelity imaging with phased ALMA in Bands 1 and 3 as part of VLBI arrays will produce better reconstructions of the jet emission, allowing observers to more accurately model the structure in both the forward jet and counterjet to determine whether the intrinsic structure is indeed asymmetric.

#### 4.5. Internal Jet Structure

Models of BL Lac objects with TeV emission are self-inconsistent on the Doppler factor of the jet, which Henri & Saugé (2006) refer to as the “bulk Lorentz factor crisis of TeV blazars.” In brief, the two broad humps in the spectral energy distributions of these objects are usually attributed to synchrotron self-Compton (SSC) and inverse Compton processes associated with relativistic leptons. The fact that TeV photons are detected—and therefore not destroyed by pair production processes—and the timescale of variability lead to the conclusion that the bulk Lorentz factor must be very high (e.g., 10 to 50) in the SSC region. However, BL Lac objects are a small subset of a larger class of FR I galaxies in which the jet is not aligned with the line of sight. The statistics imply that the bulk Lorentz factor of the BL Lac subset should be close to 3, about an order of magnitude lower than believed from SSC/TeV arguments.

One possible resolution is if the jet is composed of two different regions, a mildly relativistic jet containing and confining a pair plasma. This model predicts that the jet emission at 3 mm, where opacity effects are less severe than at centimeter wavelengths, should be limb-brightened at a distance of  $\sim 1000 r_{\text{Sch}}$  from the black hole. Polarimetric and spectral index observations support the existence of spine/sheath structures in some jets (e.g., Attridge et al. 1999; Aaron 1999; Edwards et al. 2000). Typical jet sources at nearby redshift ( $z < 0.1$ ) are relatively weak, though, with flux densities less than 1 Jy at 86 GHz. In one epoch, GMVA observations of the TeV BL Lac source Markarian 501 revealed what appears to

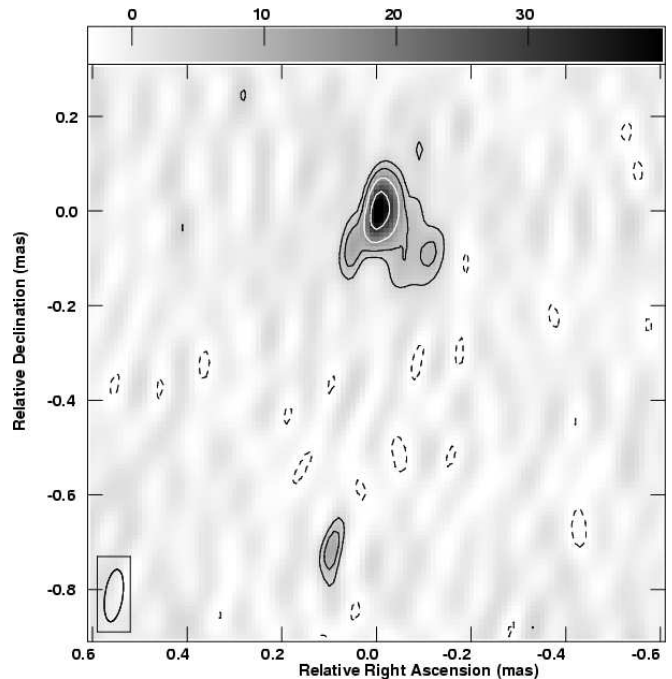


FIG. 12.— The 3 mm map of Mrk 501 (Giroletti et al. 2008) is suggestive of limb-brightened structure on scales of  $\sim 1000 r_{\text{Sch}}$ , as predicted by two-component jet models, but the image fidelity provided by the GMVA alone is not sufficient to be conclusive.

be limb-brightened jet structure on the relevant spatial scale (Figure 12; Giroletti et al. 2008). However, the image fidelity is poor, and later observations in good observing conditions were unable to confirm the result (Koyama et al., in prep.). This indicates that existing instrumentation may just barely be able to reveal features of great interest, but improvements in sensitivity and image fidelity, as would be provided by including phased ALMA in Band 3 VLBI observations, are necessary for a real breakthrough.

#### 4.6. Polarization and Magnetic Fields

Full-polarization VLBI observations at high frequencies have important advantages in the study of AGN jets. Faraday rotation and depolarization effects are reduced at higher frequencies. Due to synchrotron self-absorption, the observed emission at millimeter wavelengths comes from closer to the jet base. The polarized emission tracks the magnetic field, which plays a crucial role in jet formation and collimation, from the neighborhood of the black hole up to extragalactic distances (e.g., Broderick & Loeb 2009; Homan et al. 2009; Gómez et al. 2011; O’Sullivan et al. 2011; Tchekhovskoy et al. 2011; McKinney et al. 2012). Polarimetric VLBI observations can probe the strength (e.g., Savolainen et al. 2008; O’Sullivan & Gabuzda 2009) and spatial structure of the magnetic fields and can therefore be used to test theories of jet structure. For instance, if the spine of the jet is pressure dominated but confinement is provided by toroidal magnetic fields, the gradient of Faraday rotation across the jet should have a constant sign along the jet direction (Blandford 2008). Indeed, such rotation measure gradients have been detected in several jets (e.g., Asada et al. 2002; Gabuzda et al. 2004; Gómez et al. 2008; Hovatta et al. 2012) and interpreted as indicating the presence of a toroidal or helical magnetic field in the jet sheath. However, the region in which the rotation measure gradient is detected is located at more than  $10^5 r_{\text{Sch}}$  from the black hole, beyond the acceleration and collimation zone. High angular resolution observations with high sensitivity and image fidelity would allow similar results to be obtained nearer to the central black hole.

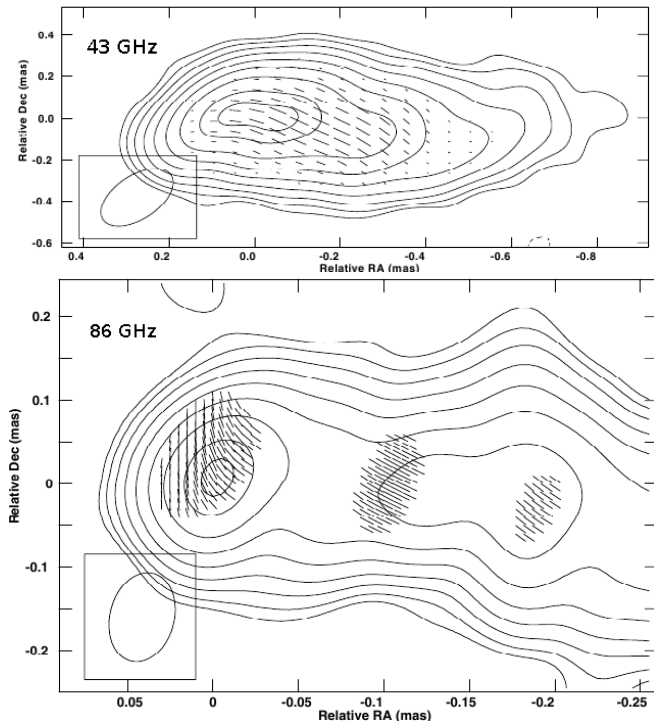


FIG. 13.— Polarization maps of 3C 345 at 43 GHz (Jorstad et al., in prep.) and 86 GHz (Martí-Vidal et al. 2012). The very compact polarized region close to the core at 86 GHz, whose electric vectors are rotated by almost 90 degrees with respect to the rest of the jet, is not detectable at 43 GHz, possibly due in part to beam depolarization.

The inclusion of phased ALMA will dramatically improve polarization capability at millimeter wavelengths. The quality and purity of the polarization signal in the ALMA receivers will allow dramatic increases in the fidelity of full-polarization VLBI images at high frequencies, which can be the limiting factor for polarimetric imaging at 86 GHz; for example, the noise cutoff can exceed 50% of the polarization peak in current GMVA observations (Martí-Vidal et al. 2012). The large collecting area is also critical for improving the sensitivity of millimeter VLBI arrays, since the polarized flux is generally only a small fraction (often 10% or less) of the total intensity signal. The higher angular resolution available on long baselines to ALMA is important for reducing beam depolarization, which reduces sensitivity to structures that vary in polarization position angle on scales comparable to the beam size (Figure 13).

#### 4.7. Jet Precession and Binary Black Holes

Many AGN jets are observed to exhibit swings in the position angle of the inner jet (e.g., Stirling et al. 2003; Tateyama & Kingham 2004; Agudo et al. 2007). Multiple hypotheses have been advanced to explain jet precession, including binary black hole systems (Begelman et al. 1980), accretion disk instabilities, and the Bardeen-Petterson effect (Caproni et al. 2004 and references therein). Progress on understanding which mechanisms apply to specific cases has been unsteady. For example, the periodic regular outbursts in OJ 287 have been explained as arising due to interactions of a binary pair of SMBHs (Sillanpää et al. 1988). Although this model has been developed and refined over the past two decades, no model is consistent with the totality of the observational evidence, including the timing of the outbursts, radio imaging, and optical polarimetry (Villforth et al. 2010). In some sources, there is no consensus even as to whether or not the jet precession is periodic (e.g., Mutel & Denn 2005). Regular monitoring with high angular resolution and high sensitivity is required to clarify the observational picture, a necessary pre-

requisite for interpretation. The mechanisms producing precession in binary AGN systems with accretion disks may also have applicability to Galactic microquasars (e.g., Katz 1997).

Supermassive binary black holes, which form during major galactic mergers, are predicted to evolve to a close pair and subsequently coalesce. Clear evidence exists for nearby interacting galaxies with jets as well as for black holes with separations on scales from kiloparsecs down to parsecs (Owen et al. 1985; Komossa et al. 2003; Rodriguez et al. 2006; see also review in Komossa 2006). Binary black hole systems may spend a large fraction of their lifetime at subparsec scales (Begelman et al. 1980), corresponding to angular scales of hundreds of microarcseconds at typical distances (Kudryavtseva 2008). The long baselines and sensitivity of phased ALMA are necessary to study the interactions within these close binary systems, such as the strength of the radio emission from close black hole pairs and the presence of a secondary jet. The presence of a second black hole causes periodic or quasi-periodic variability of the radio flux density and VLBI core flux (e.g., Qian et al. 2007, Kudryavtseva et al. 2011). Astrometry of the innermost jet of these candidate binary systems will test whether the black holes follow elliptical trajectories around a common mass center, providing the first direct evidence that these systems do indeed contain more than one supermassive black hole.

#### 4.8. Microquasars

Microquasars have emerged as very important local analogues of AGN. They represent an opportunity to observe black hole dynamics and jet formation on a much smaller scale. ALMA will open up an important new way to study these because the field is currently limited by the need to go to higher frequencies for better resolution and sensitivity.

Microquasars are the stellar remnant of a star that has collapsed to form a compact object, such as a neutron star or black hole, and has remained gravitationally bound to its binary companion star. Matter is transferred from the companion star to the compact object either via a stellar wind (for high-mass stars) or a Roche lobe (for low-mass stars). An accretion disk forms around the compact object, releasing extremely high energies within a very small volume. Microquasars release a small fraction of the inflow matter by accelerating particles into highly collimated bipolar jets; hence they have a similar morphology to quasars, but on much smaller scales.

Like AGNs, the jets from microquasars have a high luminosity, nonthermal spectra, and polarization properties consistent with self-absorbed synchrotron radiation (Hjellming & Johnston 1988). The minimum size of the jet region is related to the mass of the compact object and the turnover frequency at which the emission transitions from being self-absorbed to optically thin:  $\nu_{\max} \propto r_{\min}^{-1} \propto M_{\text{BH/NS}}^{-1}$ . Therefore, emission from the compact jet can dominate the SED from stellar-mass sources at much higher frequency than in the cores of AGN (e.g., SS433; Figure 14). While we know that shocked ejecta from these sources can have superluminal apparent motion (Dhawan et al. 2000), the velocity of the compact jet is still unknown. We do not know exactly where superluminal shocks are formed or how their formation time is associated with changes in the accretion disk.

One of the most persistently bright Galactic microquasars is GRS 1915+105, which appears to be in near constant outburst. It is estimated that the source has a relatively high accretion rate ( $\sim 0.1 L_{\text{Edd}}$ ), which feeds a jet moving at up to  $0.98c$  (Mirabel & Rodríguez 1994; Fender et al. 1999), giving an overall spectrum that is flat and bright ( $> 100$  mJy) from radio to submillimeter wavelengths. Moreover, the source has

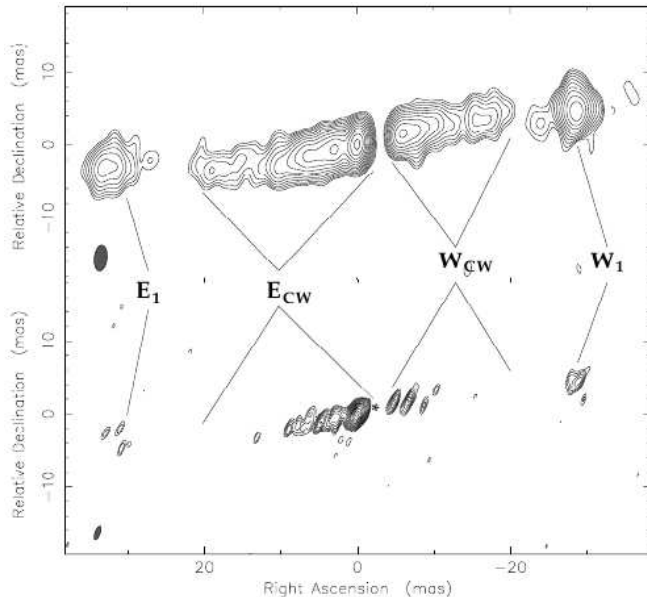


FIG. 14.— Images of the jet in SS433 at 5 GHz (upper image) and 15 GHz (lower image), from Paragi et al. (1999).

one of the largest accretion disks in the Galaxy. With an estimated outer radius of  $10^{12}$  cm (Done et al. 2004), the disk size corresponds to an angular scale of  $\sim 10 \mu\text{as}$ , assuming a distance of 10 kpc. This matches very well the angular resolution of VLBI baselines to phased ALMA at millimeter and submillimeter wavelengths. VLBI with phased ALMA will be able to directly resolve the accretion disk and image the region where the particles are accelerated to superluminal apparent velocities. It will be possible to measure the expansion of the shocked jets, measure the tangential jet cross-section, and pinpoint the position of the central black hole or neutron star.

ALMA will also be able to study the proposed free-free absorption region and observe anisotropy in the stellar wind around high-mass stars such as Cygnus X-1 (Brocksopp et al. 2002). Located at a distance of 1.86 kpc (Reid et al. 2011), the black hole X-ray binary Cyg X-1 is observed to transition between low/hard and high/soft X-ray states. It is theorized that these states are characterized by the existence of a thick advection dominated accretion flow (ADAF) inside a transition radius and a geometrically thin disk with hot corona outside this radius (Narayan 1996). The low/hard and high/soft states may represent the two extremes of this picture, with the system transitioning from an ADAF into a thin disk as the accretion rate increases (Esin et al. 1998). Simultaneous radio and X-ray monitoring suggests that the disk, corona, and jet are all coupled, with the location of the jet base around  $20 GM/c^2$  above the black hole rather than near the inner edge of the accretion disk (Miller et al. 2012). Cyg X-1 is seen to produce a radio jet extending out to about 15 mas (e.g., Stirling et al. 2001), but, unexpectedly, VLBI observations at centimeter wavelengths do not provide any evidence for the formation of knots or shocks as Cyg X-1 transitions between the low/hard and high/soft states (Rushton et al. 2012). Nevertheless, some differences must exist between the jet in these two states, since the total radio flux is modulated by the orbital period (5.6 days; Pooley et al. 1999) in the low/hard state but not in the high/soft state (Rushton et al. 2012); furthermore, the millimeter flux density is substantially higher in the high/soft state than in the low/hard state (Tigelaar et al. 2004). It is possible that structural changes in the jet are being masked by the high optical depth near the radio core at centimeter wavelengths, although the very flat spectrum from radio through

millimeter wavelengths suggests that a combination of self-absorbed synchrotron, free-free, and thermal emission combine to produce the emission from Cyg X-1 (Fender et al. 2000). High-resolution VLBI observations in Bands 1, 3, and 6 including phased ALMA will have a much greater capability of detecting jet changes during the transition between the hard and soft states. Due to their rapid timescale of variability, microquasars such as Cyg X-1 represent unique probes of structural changes in small-scale disk-corona-jet systems, but the same physical processes may be applicable to AGN/jet systems as well, in which variability due to changes in the accretion rate occur much more slowly.

Finally, the inclusion of ALMA in VLBI arrays will enable high-precision astrometry (§ 8) of X-ray binaries. Parallax measurements provide a direct geometric distance to the source, an important prerequisite for extracting the masses of the objects in these systems (see, e.g., Orosz et al. 2011). Detections of the orbital motion of the jet base place strong constraints on physical properties of the binary system, including estimates of the semimajor axis of the orbit and the ratios of the masses in the system. Cyg X-1 serves as a good example of the power of these techniques (Reid et al. 2011; Orosz et al. 2011), but the size of the orbital motion in angular units ( $\sim 70 \mu\text{as}$ ) is larger than most other X-ray binaries. The extra resolution provided by VLBI with phased ALMA in Bands 1 and 3 may be necessary for other sources.

## 5. PULSARS

Pulsars are broadband, steep-spectrum radio sources. Pulsars are typically observed at frequencies of a few GHz because the timing precision scales with S/N while the effects of the interstellar medium become less severe at higher frequencies (e.g., Lorimer & Kramer 2005). A number of pulsars are strong enough for individual pulses to be detected even at frequencies above 10 GHz (Xilouris et al. 1994), providing clues for identifying the as-yet unknown origin of the coherent emission process of pulsars (Lorimer & Kramer 2005). It is the quest for solving this “pulsar emission mystery” that is one of the main motivations for pulsar observations at very high frequencies. The highest frequency at which a radio pulsar (PSR B0355+54) has been observed to date is 87 GHz, using the IRAM 30-m telescope (Morris et al. 1997). Being able to study pulsars at millimeter wavelengths is also important for our understanding of the relationship between neutron star populations and for the search for pulsars in the Galactic Center region. Detecting a pulsar in orbit around Sgr A\* would allow astronomers to measure the properties of the central SMBH with unprecedented precision.

### 5.1. Deciphering the Emission Mechanism

A number of pulsars have been detected at millimeter wavelengths: nine sources at 32 GHz, four at 43 GHz, and one at 87 GHz (see Löhmer et al. 2008 for a recent summary). A sensitive millimeter telescope is needed to increase this number. The location of ALMA is especially appropriate, since 72% of all known pulsars are located in the Southern hemisphere.

Previous observations indicate that the emission properties at these very high frequencies are particularly interesting for understanding the creation of coherent pulsar emission. Two out of the nine sources detected above 30 GHz show a peculiar change in the flux density, indicating a flattening or even an increase in the flux density with increasing frequency (Kramer et al. 1996; Löhmer et al. 2008). This change in the spectrum was not unexpected, since it has been known for a long time that the Crab pulsar’s infrared flux density is much higher than the high-frequency radio flux density (Lyne & Smith 2005). A similar result comes from observations of the Vela pulsar

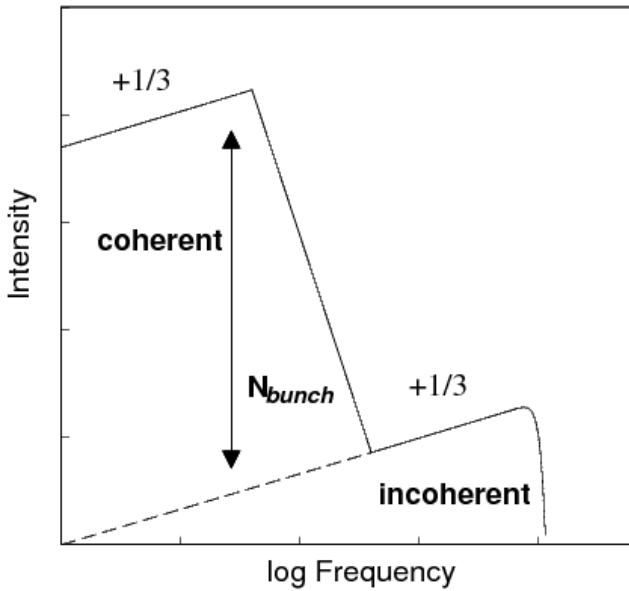


FIG. 15.— Idealized spectrum expected for curvature emission from bunched particles (adapted from Michel 1982, 1991) as an example of the transition from coherent to incoherent emission (Kramer 1995). In this case, the coherent radiation is enhanced with respect to the incoherent emission by a factor corresponding to the number of particles within a bunch.

(Danilenko et al. 2011). One natural interpretation for a spectral change in the range between centimeter and infrared observations is that the coherence conditions for normal pulsar radio emission break down and an incoherent component of the emission takes over (Kramer 1995; Michel 1982, 1991). Indeed, many of the poorly-understood (though well-studied) striking properties of the radio emission are likely a consequence of the coherence process, including nanosecond-scale pulse structure, very high brightness temperatures exceeding  $10^{36}$  K, linear polarization fractions approaching 100% (often with a strong circularly-polarized component), and steep radio spectra with spectral indices ranging between 0 and  $-3.4$ . As plasma moves along curved magnetic field lines in the magnetosphere, there should always be an underlying incoherent component that could become detectable once the coherence condition breaks down (Figure 15).

The intrinsic coherence length could be determined by detecting this break in the spectrum, providing invaluable clues to understanding the emission process. Phased ALMA would allow the first systematic study of pulsars at frequencies of 90 GHz or higher. With 50 antennas, phased ALMA could reach an equivalent continuum flux density of  $8.8 \mu\text{Jy}$  in 1 hr at 92 GHz, detecting PSR B0355+54 easily with  $S/N \approx 60$  and PSR B1929+10, one of the two pulsars with indications for a spectral turn-up at high frequency, with  $S/N > 20$ . Assuming an average spectral index of  $-1.6$ , 3% of all known pulsars could be studied with one hour of integration, and almost 10% with a five-hour integration time. This would result in the detection of nearly 100 pulsars, providing excellent statistics for the study of emission processes at ALMA Band 3 frequencies.

### 5.2. Magnetars and Their Relationship to Pulsars

Magnetars are a special class of neutron stars that typically have rotation periods between 5 and 12 s. They get their name from their very large inferred magnetic fields (in excess of  $10^{14}$  G), which appear to power these sources during their high-energy outbursts. Their radio brightness seems to be a transient event that may be related to or even triggered by the high-energy outburst (Camilo 2008). When radio-bright,

magnetars show similarities to pulsars but retain important differences: they are very highly linearly polarized, show an unusually large degree of variation in their pulse shape, and have a very flat and variable flux density spectrum (Camilo et al. 2008; Kramer et al. 2007). The magnetar XTE J1810-197 has been detected with the IRAM 30-m telescope at a frequency as high as 144 GHz with a flux density of about 1.2 mJy (Camilo et al. 2007). Studies of magnetar properties would therefore be easily possible with phased ALMA and should allow comparison of magnetar and radio pulsar properties, advancing understanding of radio-emitting neutron stars in general. In particular, there are questions of why the radio spectrum of magnetars is so flat and to what frequencies it could extend.

### 5.3. Probing the Spacetime Around Sgr A\*

Pulsars in orbit around Sgr A\* will be superb probes to study the properties of the central SMBH (e.g., Wex & Kopeikin 1999; Liu et al. 2012). Timing observations of such pulsars complement VLBI imaging for testing general relativity because the two techniques are based on different and independent observables. Finding a normal, slowly-rotating pulsar in a reasonable orbit around Sgr A\* could under ideal circumstances measure the mass of the black hole and test the cosmic censorship conjecture and no-hair theorems to high precision (Liu et al. 2012). Finding pulsars in the Galactic Center will provide invaluable information about the Galactic Center region itself. The characteristic age distribution of the discovered pulsars will give insight into the star formation history. Millisecond pulsars can be used as accelerometers to probe the local gravitational potential. The dispersion and scattering measures and their variability can serve as probes of the distribution, clumpiness, and other properties of the central interstellar medium. Faraday rotation can provide measurements of the central magnetic field.

Given the huge rewards for finding and timing pulsars in the Galactic Center, various efforts have been conducted to survey the inner Galaxy (Kramer et al. 2000, Johnston et al. 2006; Deneva et al. 2009; Macquart et al. 2010). None of these efforts has been successful, despite the expectation to find more than 1000 pulsars in the Galactic Center region, including millisecond pulsars (e.g., Wharton et al. 2012) and highly eccentric systems including both a stellar black hole and a millisecond pulsar (Faucher-Giguère & Loeb 2011). However, finding these pulsars is incredibly difficult due to the severely increased interstellar scattering produced by the highly turbulent medium in the vicinity. Scattering leads to pulse broadening that cannot be removed by instrumental means and that renders the source undetectable as a pulsar, in particular if the scattering time exceeds a pulse period. The scattering time is a strong function of frequency (Lorimer & Kramer 2005), so the aforementioned pulsar searches have been conducted at ever-increasing frequencies—the latest being conducted around 20 GHz. The difficulty in finding pulsars at these frequencies is two-fold. First, the flux density is significantly reduced due to the steep spectra of typical pulsars. Second, the reduced dispersion delay, which needs to be removed but also acts as a natural discriminator between pulsar signals and terrestrial interference, makes verification of real signals difficult.

Recording baseband data with the ALMA beamformer will help in both respects. ALMA's sensitivity and location in the Southern hemisphere will enable deep pulsar searches of the Galactic Center. The baseband data can be used to study the frequency structure of the signal in great detail, for instance, by synthesizing a very fine polyphase filterbank or searching directly for chirped signals. The scattering and dispersion

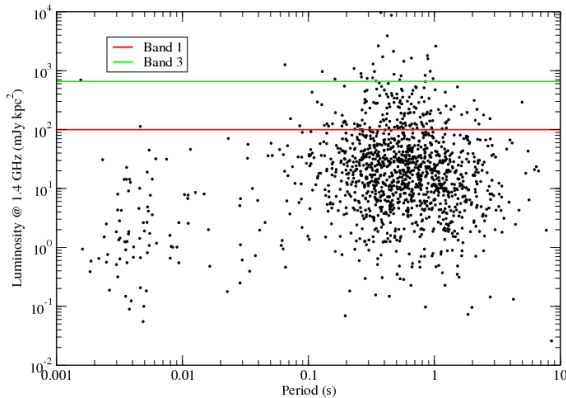


FIG. 16.— Luminosity of the known radio pulsar population. The survey sensitivity of searches with ALMA Bands 1 and 3 are indicated with red and green lines, respectively. These limits were derived using a distance of 8.5 kpc to the Galactic Center and assuming an average spectral index of  $-1.6$ .

times are low enough at ALMA frequencies that it will be possible to detect even millisecond pulsars at Band 3. Scaling from the properties of known pulsars, a search with 50 phased ALMA dishes would detect pulsars with a 1.4 GHz luminosity of about 100 mJy kpc<sup>2</sup> at Band 1 and 660 mJy kpc<sup>2</sup> at Band 3 (Figure 16). High-frequency pulsar searches could be done commensally with other observations. For instance, the same data taken for Band 6 VLBI observations or routine ALMA Band 3 observations of the Galactic Center could be used for pulsar searches, thus leveraging the same ALMA observing time for two different scientific purposes. Indeed, the recent serendipitous detection of a young pulsar in the vicinity of the Galactic Center (Eatough et al. 2013) provides evidence in support of a yet-undetected population of pulsars near Sgr A\*.

## 6. GRAVITATIONAL LENS SYSTEMS AND ABSORPTION AT COSMOLOGICAL DISTANCES

### 6.1. Dark Matter

Foreground galaxies may gravitationally lens high-redshift galaxies or AGN into multiple images. If small-scale overdensities are present within the dark matter halo of the lensing galaxy, secondary magnifications and distortions of the separate images can also occur (see review in Zackrisson & Riehm 2010). Whereas morphological features intrinsic to the source will be present in all images, lensing due to dark halo substructure will produce uncorrelated effects in the images (e.g., Inoue & Chiba 2005). Searches for such small-scale lensing effects can probe the dark subhalos predicted by standard cold dark matter (CDM) simulations or more compact forms of halo substructure produced in alternative structure formation scenarios, such as primordial black holes or ultracompact minihalos. This is particularly interesting in the dwarf-galaxy mass range, where the subhalos seen in CDM simulations greatly outnumber luminous satellite galaxies, suggesting that a vast population of extremely faint or completely dark subhalos may be awaiting detection in the halo of every large galaxy. The superior resolution and sensitivity provided by VLBI with phased ALMA will constrain halo substructure at lower masses than previously possible. Observations of lensed AGN jets in Band 3 would allow for the detection of black holes with masses of  $\sim 10^3$ – $10^6 M_{\odot}$  or ultracompact minihalos with masses of  $\sim 10^6$ – $10^8 M_{\odot}$  (Zackrisson et al. 2013). Strongly lensed submillimeter galaxies can, due to their larger intrinsic sizes ( $\sim 100$  pc; Swinbank et al. 2010), be

used to probe lower-density substructures, and observations in Band 7 could make standard CDM subhalos detectable down to at least  $\sim 10^7 M_{\odot}$ .

### 6.2. Absorption

Most potential VLBI targets require very high brightness temperatures to be detected. In the case of spectral-line VLBI, maser amplification is required to produce sources that can be detected through their own emission. On the other hand, molecular gas can also be seen in absorption when back-lighted by strong background quasars. Using this technique, spectral-line VLBI provides the possibility to observe molecules even in distant galaxies. The canonical example of a molecular absorption system is found toward PKS 1830–211, a lensed radio-loud quasar at  $z = 2.5$ . A spiral galaxy at redshift  $z = 0.886$  lies along the line of sight, allowing molecules to be detected at this intermediate redshift (Wiklind & Combes 1996). Muller et al. (2011) detected 28 different molecules and 8 isotopologues in this system (Figure 17), which they note is the extragalactic source with the largest number of detected molecular species, making it possible to undertake detailed studies of molecular and isotopic abundance ratios in a source at a cosmological redshift.

High angular resolution is important in order to reduce the volume of gas being observed, which can blend multiple subregions with differing velocities, abundances, and excitation values. The spatial distribution on milliarcsecond scales of cosmologically distant absorbers has been determined in a couple of systems (e.g., Carilli et al. 2000). In the case of PKS 1830–211, monitoring of the HCO<sup>+</sup> and HCN line profiles reveals that the clouds producing the absorption have sizes smaller than 1 pc (Muller & Guélin 2008). Present VLBI observations at 43 GHz do not resolve the source, although Jin et al. (2003) estimate a size of  $1.8 \times 1.2$  pc for the southwest lensed image after deconvolution of their observing beam. High-resolution observations of HC<sub>3</sub>N in this system show that the spatial distribution of two different transitions on these scales is different, with the transitions being offset from both the continuum peak and each other (Figure 18; Sato et al. 2013). The implied rotational temperature is lower than the expected cosmic microwave background (CMB) temperature at the absorber’s redshift, which may be due to unabsorbed continuum emission within the observing beam. By observing multi-transitions from multiple species in the millimeter band, Muller et al. (2013) could derive a precise and accurate measurement of the CMB temperature toward PKS 1830–211. They found a value in agreement with the expected value at the redshift of the absorber, consistent with adiabatic expansion of the Universe. Similar observations of other absorber sources could explore the evolution of the CMB temperature with redshift, shedding light on the nature of dark energy.

Molecular absorption systems can also be used to place constraints on the cosmological variations of fundamental constants of nature, like the fine structure constant ( $\alpha$ ) or the proton-to-electron mass ratio ( $\mu$ ), as an important test of fundamental physics (e.g., Uzan 2011). The rest frequency of some spectral lines have different dependences on fundamental constants. If these constants vary with space and/or time (in contradiction to the invariance principle), then the frequency of such lines will appear to drift and offset in velocity with respect to other reference transitions. Since kinematic Doppler shifts can mimic the apparent frequency shifts that would be produced by variations in fundamental constants, it is preferable to observe lines that arise from cospatial species, or from a single suitable species like methanol (Bagdonaite et al. 2013).

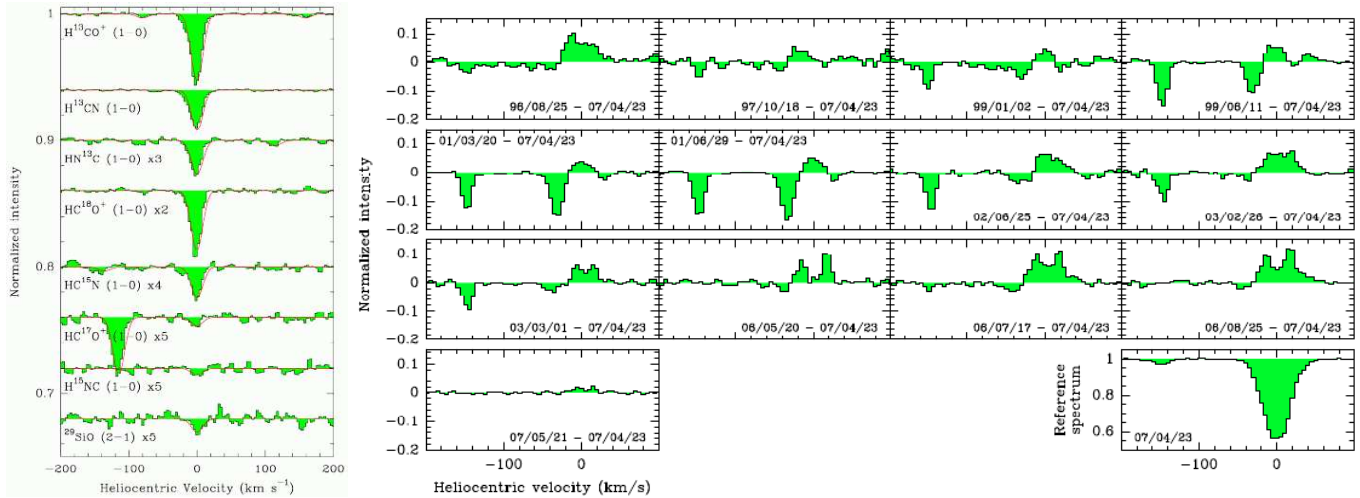


FIG. 17.— Molecular absorption in the absorbing system toward PKS 1830–211. Many molecular species and isotopologues are detected in the millimeter regime in this system (left, Muller et al. 2011). Their variability indicates the the absorbing clouds are very compact (right, Muller & Guélin 2008).

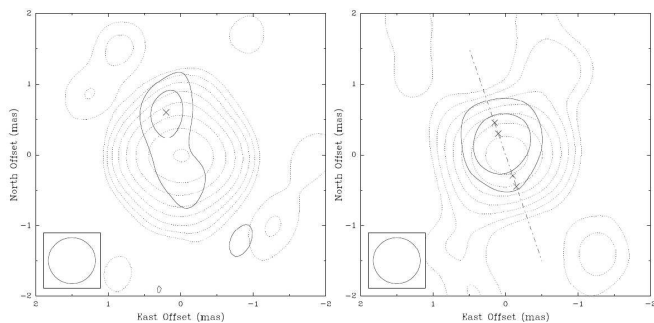


FIG. 18.— There is structure in the submilliarcsecond distributions of the  $J = 3 \leftarrow 2$  (left, solid contours; dotted contours show the continuum emission from the background quasar) and  $J = 5 \leftarrow 4$  (right) of  $\text{HC}_3\text{N}$  in PKS 1830–211 that is not fully resolved by the observing beam at centimeter wavelengths (Sato et al. 2013). High-frequency VLBI with ALMA will improve substantially on the resolution available with current VLBI networks.

VLBI with ALMA in Band 6 will improve on the angular resolution in this system by a factor of more than 30 in solid angle, likely substantially reducing velocity scatter between molecular transitions due to contributions from different clouds in the absorbing galaxy. This will be vitally important for improving estimates of the deviation of  $\mu$ . Henkel et al. (2009) measure  $|\Delta\mu/\mu| = (+0.08 \pm 0.47) \times 10^{-6}$  from observations of a range of different transitions of  $\text{NH}_3$  and  $\text{HC}_3\text{N}$ , but the rms velocity variation within transitions of each species is nearly  $1 \text{ km s}^{-1}$ , producing a  $0.5 \text{ km s}^{-1}$  random uncertainty in the average velocities of the two species. Muller et al. (2011) found a comparable scatter in the centroid velocities of their large number of different species. Therefore, it is essential to obtain sensitive VLBI observations to reduce the systematic uncertainty in  $\Delta\mu/\mu$  due to kinematic and chemical segregation in the absorbing clouds. Arrays with baseline lengths on G $\lambda$  scales, such as millimeter VLBI arrays including ALMA, will be able to resolve these clouds and even smaller structures, reducing systematic errors in fundamental constant variation tests. The sensitivity provided by phased ALMA may allow the extension of this technique to as-yet-undetected weaker absorber systems.

The detection of rare isotopologues in distant galaxies also offer the possibility to investigate the nucleosynthesis history in the Universe from the evolution of isotopic ratios. For example, Muller et al. (2006, 2011) could estimate the isotopic abundance ratios of carbon, nitrogen, oxygen, sulfur and silicon at  $z=0.89$  toward PKS 1830–211, at a time roughly half the current age of the Universe. They found significant differ-

ences compared to the same isotopic ratios in the local Universe, and interpreted them as due to a gradual nucleosynthesis enrichment by low-mass stars, while massive stars contribute on a much smaller timescale. With high-angular resolution and high sensitivity, offered by the VLBI network including ALMA, it would be possible to investigate the interstellar mixing of elements at the sub-parsec scale in distant galaxies, and to much smaller scales by studying molecular absorption in Milky Way clouds.

Finally, recent ALMA Early Science data on PKS 1830–211 focusing on absorption lines in the intervening galaxy have revealed remarkable time- and frequency-dependent variations in the flux ratios between the two lensed images of the background blazar (Martí-Vidal et al. 2013). Those variations were interpreted as chromatic structure changes related to the activity close to the base of the blazar jet, as the ALMA observations were serendipitously coincident with a strong gamma-ray flare in the blazar. Hence, the observations of molecular absorbers have multiple interests, from the study of absorbing gas in the foreground galaxy, using molecules as cosmological probes, to the study of the background (most likely strongly lensed) quasar, vitally requiring the high angular resolution and high sensitivity that ALMA will bring to VLBI.

## 7. MASERS

Thanks to large amplification factors, many masers are very spatially compact. Multi-epoch VLBI studies of masers have been very scientifically productive, allowing astronomers to understand the environments and detailed dynamics of star-forming regions (SFRs) and the envelopes of evolved stars as well as obtain robust geometric distance measurements of other galaxies and of SFRs in the spiral arms of the Milky Way. The main emphasis has traditionally been placed on observations at centimeter wavelengths (OH and  $1.35 \text{ cm H}_2\text{O}$ ), but there has been growing interest in millimeter and submillimeter maser studies as sensitive high-frequency telescopes and arrays have come on line (e.g., Humphreys 2007). These bands provide access to additional transitions of masing species commonly observed at centimeter and millimeter wavelengths (e.g., SiO,  $\text{H}_2\text{O}$ ), as well as new maser transitions that have been less well studied, particularly with high spatial resolution (e.g., HCN). Two major species observed in both SFRs and circumstellar environments,  $\text{H}_2\text{O}$  and SiO, exhibit masing transitions in ALMA Bands 3 and 5–9, with other observed or predicted maser transitions existing in most of the remaining ALMA Bands.

### 7.1. Galactic Science

The spectrum of silicon monoxide and its isotopologues includes transitions at multiples of approximately 43 GHz, many of which are observed to produce masers in stellar envelopes. The 43 and 86 GHz transitions of SiO are routinely observed using VLBI techniques, and the millimeter and submillimeter bands provide access to a number of high rotational and vibrational SiO transitions detectable in evolved stars (e.g., Wittkowski et al. 2011). For example, successful VLBI observations of SiO masers at 129 GHz have been performed in the envelope of the supergiant VY Canis Majoris (Doeleman et al. 2002), and multiple SiO transitions have been imaged in a single object (e.g., Soria-Ruiz et al. 2004).

In general, different maser transitions in a molecules and its isotopologues probe different physical conditions and thus different regions within a given source. The simultaneous observation of multiple transitions therefore enables mapping of the gas kinematics as well as changes in parameters such as density and temperature as a function of radius. The high sensitivity of phased ALMA, together with its rapid band switching and subarraying, will allow much more accurate registration of maser maps in different transitions, as well as the study of the origin of emission that, present in single-dish data, is often not detected in current high-resolution VLBI maps. In the envelopes of AGB stars, detailed comparison of the ring-like distributions of different 43 and 86 GHz SiO maser transitions will provide crucial tests for constraining models of maser pumping mechanisms, as seen already in Desmurs et al. (2000), Soria-Ruiz et al. (2004, 2007), Gray et al. (2009), and in Doeleman et al. (2004) for the case of the Orion outflow.

Spatially resolved observations of high-frequency masers will also provide crucial information about magnetic fields in star-forming regions and evolved stars (Pérez-Sánchez & Vlemmings 2013). In particular, highly polarized ( $> 20\%$ ) high-frequency SiO masers are good probes of the magnetic field morphology within a few stellar radii of stellar atmospheres (e.g., Vlemmings et al. 2011). While ALMA by itself has insufficient resolution, VLBI including phased ALMA will be able to map in detail the magnetic field on very small scales. Multi-epoch observations could trace magnetic ejections from evolved stars. Although current magnetic field studies have focused on oxygen-rich stars, the 89 GHz HCN maser can be used for similar studies of carbon-rich envelopes.

In addition to magnetic field information, maser polarization provides unique constraints on maser theory models when comparing different transitions. Previous work has been limited to the 43 and 86 GHz SiO masers, and only one source has been studied in detail (Richter et al. 2012). With sensitive millimeter VLBI, many more sources and maser transitions will be available for study, and it will finally be possible to investigate predicted correlations between linear and circular polarization fractions as well as between linear polarization fractions of maser features at different frequencies.

While SiO masers are known in hundreds of late-type stars, they have been detected in only 3 high-mass SFRs: Sgr B2, W51, and Orion. SiO masers have been extensively mapped in the direction of the Orion compact source I. At centimeter wavelengths, proper motion measurements of these masers provide a unique probe of accretion and outflow processes within  $\sim 10$ -100 AU of the source (e.g., Matthews et al. 2010). Application of millimeter VLBI to the study of this source would enable more complete mapping of the material through access to numerous additional SiO transitions. The previous observations at 43 GHz with  $\sim 500 \mu\text{as}$  resolution by Matthews et al. show that, in contrast with what is observed

in late-type stars, nearly all the flux is recovered at that resolution, suggesting that the type of sensitive, higher resolution studies enabled by millimeter VLBI with phased ALMA are likely to be fruitful for improving proper motion studies and providing more detailed mapping of the gas kinematics. As in the case of evolved stars, simultaneous measurements of multiple SiO transitions surrounding Source I will also provide tests of maser excitation mechanisms (e.g., Goddi et al. 2009). Initial findings by Matthews et al. suggest these may be quite different from the case for evolved stars.

Submillimeter water masers expected in ALMA Bands 7–9 are also relevant to studies of star formation. Besides the ubiquitous 22 GHz line, strong water lines have been detected at 183, 321, and 325 GHz and higher frequencies in SFRs as well as in several circumstellar envelopes of late-type stars using single-dish telescopes (Humphreys et al. 2007 and references therein). Their spectra show spectacularly intense peak fluxes (up to 10000 Jy) and large velocity ranges (up to  $300 \text{ km s}^{-1}$ ). Neufeld & Melnick (1991) and more recently Daniel & Cernicharo (2013) discussed collisional pumping for these masers and predicted simultaneous inversion of 22, 321, and 325 GHz and other submillimeter H<sub>2</sub>O transitions over a wide range of physical conditions. Recent ALMA science verification observations have produced the first detection of high-excitation 232.686 GHz water masers associated with Orion KL Source I (Hirota et al. 2012), a vibrationally excited masing transition that, like SiO masers, was known to be excited in late-type stars; this is the first detection in a SFR. In principle, observations of different maser line ratios may be used to constrain physical conditions; in practice, this has not been possible so far because single-dish antennas and connected-element interferometers can only describe the average emission of many maser clumps. VLBI images of submillimeter H<sub>2</sub>O maser lines are required to provide high enough angular resolution to resolve these clumps, constraining and testing radiative transfer models and mapping gas temperature and density with high accuracy and resolution around young stellar objects.

So far, only two SFRs, Orion KL and Cep A, have been imaged in submillimeter H<sub>2</sub>O lines with the SMA. Challenging weather requirements (especially at 325 GHz) and poor dynamic range have prevented imaging of other SFRs, limiting their use as probes of high-mass star formation. ALMA's superb high site meets weather requirements for observations at 321 and 325 GHz as well as for even higher-frequency transitions of interest in SFRs and late-type stars (e.g., 439 and 471 GHz). Inclusion of ALMA in submillimeter VLBI arrays will enable studies of submillimeter H<sub>2</sub>O maser lines in a larger sample of SFRs and permit comparison with centimeter lines observed at submilliarcsecond resolution. Polarimetric observations of maser lines can also provide measurements of magnetic fields in outflows in SFR outflows (H<sub>2</sub>O masers) and in circumstellar envelopes (SiO, HCN, and H<sub>2</sub>O).

Lastly, VLBI with phased ALMA could open an entire new domain for the study of the envelopes of carbon stars, where HCN masers are believed to play a role analogous to those of SiO masers in oxygen-rich stars (e.g., Izumiura et al. 1995). This has remained until now a relatively unexplored area owing to the lack of availability of sensitive millimeter and submillimeter VLBI facilities.

### 7.2. Extragalactic Science

Luminous extragalactic masers, namely the “megamasers,” are mainly produced by two molecules: OH and H<sub>2</sub>O. While OH megamasers are in most cases related to particularly high star formation in (ultra)luminous infrared galaxies, water megamasers are associated with AGN activity, either with

accretion disks, nuclear outflows, or radio jets (e.g., Lo 2005; Tarchi 2012).

Extragalactic water masers are very compact and luminous. The canonical example of a circumnuclear water maser source, NGC 4258, contains 1.35 cm water masers embedded in a warped accretion disk around a supermassive black hole (Miyoshi et al. 1995). The Keplerian rotation of this disk as traced by the masers allows a purely geometric distance to be obtained (Herrnstein et al. 1999). The phenomenal success of modeling NGC 4258 is the inspiration for the Megamaser Cosmology Project (e.g., Reid et al. 2009b, 2013; Kuo et al. 2011), which has identified over 100 galaxies hosting megamasers to which this technique can be applied in order to measure the Hubble constant directly.

While the main focus has been on the 22 GHz transition that is easily accessible with existing VLBI arrays, millimeter and submillimeter water masers are also being targeted. These higher-frequency masers may allow the back side of the circumnuclear disk to be observed, since the disk is optically thick at 22 GHz; would provide constraints on radiative transfer models, from which the density and temperature of the disks could be inferred; and would be observable with higher angular resolution, which is important for extending the technique to more distant galaxies. One promising source is NGC 3079, a nearby Seyfert 2/LINER galaxy in which water masers have been detected at 183 and 439 GHz (Humphreys et al. 2005). Modelling of the 325 GHz line suggests that it can be inverted both under the same conditions that will produce 22 GHz masers and at lower densities and temperatures (e.g., Cernicharo et al. 2006), potentially making it an excellent probe of both the circumnuclear disk and the wide-angle outflow that may be associated with the large-scale superbubble. Cernicharo et al. (2006) find 183 GHz water masers in Arp 220—a galaxy that hosts OH megamasers but no 22 GHz water masers—which is an intriguing target for further study as water and OH megamasers are only very infrequently found in the same galaxy (Tarchi et al. 2011).

Very luminous Galactic-analogue water kilomasers are also seen in extragalactic star-forming regions (e.g., Tarchi et al. 2002; Hagiwara 2007; Surcis et al. 2009). However, some kilomasers may be related to AGN activity as well (Tarchi et al. 2011). VLBI observations of submillimeter water masers may provide an extremely high angular resolution picture of star formation in nearby galaxies as well as new insights on the putative class of nuclear kilomasers.

## 8. ASTROMETRY

Precision astrometric observations of target sources require phase connection with a nearby calibrator. The ideal case occurs when both the target and the calibrator source can be observed within the primary beam of each VLBI element. A more typical observing mode is to nod between the target and calibrator sources on a timescale faster than the atmospheric coherence time. This strategy can be employed in Band 1 and, under good weather conditions across the observing array, Band 3. At higher frequencies, where the atmospheric coherence time may be too short for nodding, astrometry could still be accomplished by observing with phased-array stations that are subarrayed to observe the target and calibrator sources simultaneously.

Astrometry is complementary to multiple aspects of jet science (§ 4). Multifrequency astrometric observations played a crucial role in identifying the location of the black hole in M87 (Hada et al. 2011) and could be extended to higher frequencies to determine the location of the 1.3 mm emission, which is associated with the inner accretion and outflow region (Doeleman et al. 2012), relative to longer-wavelength

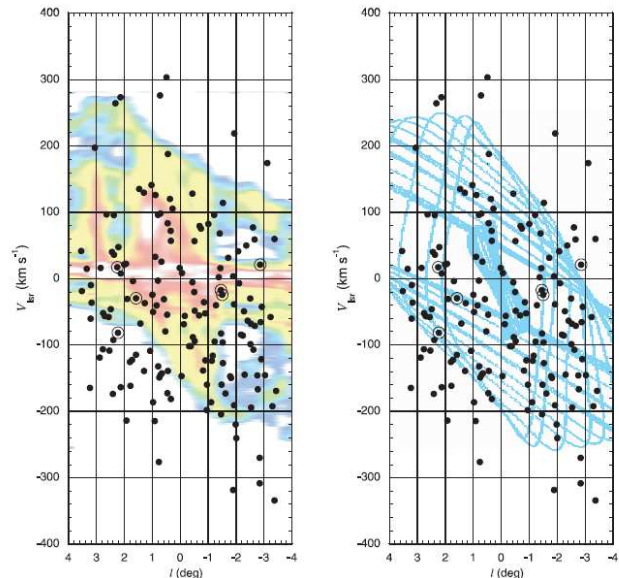


FIG. 19.— Left: Longitude-velocity diagram of SiO maser sources in the Galactic bulge, superposed atop CO line emission (Fujii et al. 2006). Right: Stellar orbits in the bar potential.

observations of the forward jet and counterjet. This would enable more accurate measurements of the jet opening angle, inclination to the line of sight, and Lorentz factor (Broderick et al. 2011c).

Sgr A\* is known to be variable across the spectrum on timescale of minutes to hours (e.g., Genzel et al. 2003; Eckart et al. 2006; Marrone et al. 2008), although it is not known which of several mechanisms may be responsible for this variability (e.g., orbiting hot spots, expansion of material ejected from the disk, or episodic ejection of material along a jet). A VLBA search for the position wander of Sgr A\* at 7 mm was able to place constraints on, for instance, the amount of the total source brightness that could be contained within an orbiting hot spot at fairly large radius ( $15 GM/c^2$ ; Reid et al. 2008), but the inclusion of phased ALMA in astrometric arrays could improve on this substantially (Broderick et al. 2011c). The proper motion of Sgr A\* has also been measured with the VLBA at 7 mm (Reid & Brunthaler 2004), but the astrometric improvements provided by the inclusion of phased ALMA in millimeter observing arrays would permit the measurement of microarcsecond-scale fluctuating components induced by stars and stellar-mass black holes in the Galactic Center (Broderick et al. 2011c). Absolute astrometric observations of Sgr A\* will also directly provide the distance to the Galactic Center,  $r_0$ , which is one of the most fundamental parameters in the field of Galactic astronomy. Lower-frequency Northern hemisphere VLBI arrays have attempted to measure the parallax of Sgr A\*, but prospects of success have been limited by severe interstellar scattering. High-frequency observations including ALMA and other stations, especially in the Southern hemisphere, will be best-suited for absolute astrometric measurements of Sgr A\*.

Astrometric observations of maser sources have been very productive in establishing geometric distances to Galactic objects and nearby extragalactic sources. For instance, centimeter-wavelength observations as part of the Bar and Spiral Structure Legacy (BeSSeL) Survey and VLBI Exploration of Radio Astrometry (VERA) have substantially revised the IAU recommended values for the Solar motion and Galactocentric Solar distance and are beginning to clarify the nearby spiral structure of the Milky Way (Brunthaler et al. 2012; Honma et al. 2012). Astrometric observations in Bands 1 and 3 of the abundant SiO masers in the Galactic bar and



nuclear region similarly have the potential to be of great help in understanding the dynamics of the inner Galaxy. In fact, there are hundreds of SiO maser sources—mostly supergiant stars—found toward the Galactic bulge and Galactic Center regions. Figure 19 shows the distribution of SiO maser sources toward the Galactic Center (Fujii et al. 2006). Some stars have a high velocity and even a forbidden velocity in terms of gas motion. This is most likely due to the bar potential; since the stars are collisionless and the gases collisional, their motions in the bar potential are expected to be different. Hence, astrometry of SiO maser sources in the bulge is complementary to astrometry with BeSSeL and VERA, which have been observing star-forming region, and will test predictions of Galactic bar models based on the three-dimensional spatial motions of stars and gas clouds. SiO maser astrometry also provides a unique opportunity to cross-register radio and infrared reference frames at submilliarcsecond accuracy (e.g., Menten et al. 1997). In addition, absolute astrometry of SiO masers in late-type stars will allow accurate alignment of maps of various maser transitions with each other, constraining the pumping mechanisms at work, and with the underlying optical star, as more accurate absolute positions are obtained with the Gaia space observatory.

Southern hemisphere VLBI arrays including phased ALMA will also be powerful for astrometry of the portion of the Galaxy inaccessible to northern arrays such as the VLBA and VERA. SiO masers in supergiant stars are again the most promising targets to reveal the structure and dynamics of the spiral structure in the third and fourth Galactic quadrants. An unbiased pilot survey of SiO masers in the southern Galactic plane using the Mopra 22-m telescope indicates that numerous suitable SiO maser target sources exist in this region (e.g., Jordan et al. 2013).

Looking beyond the Milky Way, these techniques could be used in conjunction with other VLBI-capable telescopes in the Southern Hemisphere to obtain a direct geometric distance to SiO masers in the Large Magellanic Cloud (LMC; van Loon et al. 2001), potentially improving upon Cepheid distances, which contain systematic uncertainties due to reddening and metallicity (An et al. 2007). Since SiO maser emission in the LMC is faint due to its distance, such observations cannot be done without the sensitivity provided by phased ALMA. Another application of high-precision astrometry is to measure the motions of nearby galaxies with radio AGN. A source motion of  $500 \text{ km s}^{-1}$  at a distance of 10 Mpc produces a proper motion of  $\sim 10 \mu\text{as yr}^{-1}$ . Proper motion measurements of sources in the Virgo cluster ( $\sim 16 \text{ Mpc}$ ) could be done within a few years, providing information on cluster dynamics.

Selected compact extragalactic radio sources serve as fiducial points to define the celestial reference frame. Based on several decades-long astrometric VLBI measurement time series, many of them show apparent proper motions of  $\sim 0.01\text{--}0.1 \text{ mas yr}^{-1}$ . It is crucial to understand the origin of these proper motions, to define a more accurate reference frame, and to accurately study phenomena like the secular aberration drift caused by the acceleration of the solar system barycenter due to the rotation around the Galactic center (e.g. Titov et al. 2011). While the characteristic direction of VLBI-measured AGN proper motions seems generally connected with the  $\sim 1\text{--}10\text{-mas}$  scale jet structure, there are cases of significant misalignment (Moór et al. 2011). In particular, the proper motion direction for OJ 287 is nearly orthogonal to its radio jet seen with centimeter-wavelength VLBI. The relationship between the small apparent proper motions and the brightness structure could be established with sensitive millimeter-VLBI imaging, which probes the right angular scales, well within 1 mas from the central engine.

## 9. ALMA INTERFEROMETRIC DATASETS

It is important to note that the standard operating mode for the ALMA beamformer will include archiving of the products of the ALMA Baseline Correlator. Observations with the ALMA beamformer therefore will additionally provide “regular” ALMA interferometric datasets. VLBI campaigns could end up producing deep ALMA integrations on certain targets. For example, the ALMA interferometric dataset corresponding to a series of 230 GHz VLBI observations totalling 30 hours on source would have an rms sensitivity of  $\sim 2 \mu\text{Jy beam}^{-1}$  for continuum sources and  $0.2 \text{ mJy beam}^{-1}$  for a single  $1.3 \text{ km s}^{-1}$  channel in the standard widest-bandwidth observing mode.

One field that will likely see high interest from VLBI proposers is the Galactic Center region. At 230 GHz, the ALMA primary beam of 26 arcsec covers the central parsec of the Galaxy, which includes Sgr A\*, most of the minispiral, and a portion of the circumnuclear disk. Deep continuum sensitivities will allow spectacular mapping of the morphology and polarization of the continuum emission, and spectral indices and rotation measure estimates can be determined from comparison of the measurements between the two sidebands. Variability can be probed from timescales much smaller than a single VLBI epoch to multi-epoch or even multi-year timescales, and polarimetric variability can be used to constrain changes in the Faraday rotation screen toward the Galactic Center. Flexibility with VLBI tuning at ALMA and other facilities would also permit inclusion of particular spectral lines of interest.

Deep-field ALMA datasets may be obtained in the direction of other targets based on their VLBI scientific potential. Depending on the pointing direction, these observations may contain sources in the Galactic plane or halo, nearby galaxies, and/or high-redshift galaxies. Examples of the scientific potential of these ALMA interferometer datasets can be found in the ALMA Design Reference Science Plan<sup>2</sup>.

## 10. CONCLUDING REMARKS

The preceding sections summarize areas in which the ALMA beamformer will be uniquely capable to have great scientific impact. These span a wide range: from astrophysics to fundamental physics, from Galactic sources to objects at cosmic redshift, from very compact objects to kiloparsec-scale jets, and from cool molecules to extremely hot plasmas. Most of these studies will be made possible thanks to the sensitivity and angular resolution that phased ALMA will bring to VLBI arrays. Pulsar observations with the ALMA beamformer can be done commensally with standard ALMA observing too, increasing the scientific efficiency of allocated ALMA time.

In this document we have attempted to identify the most fruitful lines of investigation that will be enabled by the ALMA beamformer. However, the history of astronomy demonstrates that when an instrument opens up a new area of discovery space, some of the most important scientific results come from unanticipated directions. The full measure of the scientific capability of the phased ALMA system will ultimately be limited only by the imagination of the astronomy community.

This work is funded by the National Science Foundation (MRI AST-1126433).

<sup>2</sup> <http://www.eso.org/sci/facilities/alma/documents/drsp.html>

## REFERENCES

- Aaron, S.E. 1999, *ASP Conf. Ser.*, 159, 427
- Abdo, A.A., et al. 2011, *ApJ*, 733, L26
- Acciari, V.A., et al. 2009, *Science*, 325, 444
- Agudo, I., et al. 2007, *A&A*, 476, L17
- Agudo, I., et al. 2011a, *ApJ*, 726, L13
- Agudo, I., et al. 2011b, *ApJ*, 735, L10
- Aitken, D.K., Greaves, J., Chrysostomou, A., Jenness, T., Holland, W., Hough, J.H., Pierce-Price, D., & Richer, J. 2000, *ApJ*, 534, L173
- Aloy, M.-A., Martí, J.-M., Gómez, J.-L., Agudo, I., Müller, E., & Ibáñez, J.-M. 2003, *ApJ*, 585, L109
- An, D., Terndrup, D.M., & Pinsonneault, M.H. 2007, *ApJ*, 671, 1640
- Antón, S., Andrei, A.H., & Taxis, F. 2012, *Mem. Soc. Astron. Ital.*, 83, 934
- Asada, K., Inoue, M., Uchida, Y., Kameno, S., Fujisawa, K., Iguchi, S., & Mutoh, M. 2002, *PASJ*, 54, L39
- Asada, K., & Nakamura, M. 2012, *ApJ*, 745, L28
- Attridge, J.M., Roberts, D.H., & Wardle, J.F.C. 1999, *ApJ*, 518, L87
- Bach, U., Krichbaum, T.P., Alef, W., Witzel, A., & Zensus, J.A. 2002, *Proc. 6th EVN Symp.*, 155
- Bagdonaitė, J., Jansen, P., Henkel, C., Bethlehem, H.L., Menten, K.M., & Ubachs, W. 2013, *Science*, 339, 46
- Bardeen, J.M., & Petterson, J.A. 1975, *ApJ*, 195, L65
- Barthel, P.D. 1989, *ApJ*, 336, 606
- Begelman, M.C. 1995, *Proc. NAS*, 92, 11442
- Begelman, M.C., Blandford, R.D., & Rees, M.J. 1980, *Nature*, 287, 307
- Begelman, M.C., Sikora, M., & Rees, M.J. 1994, *ApJ*, 421, 153
- Biretta, J.A., Junor, W., & Livio, M. 2002, *New Astronomy Reviews*, 46, 239
- Biretta, J.A., Sparks, W.B., & Macchetto, F. 1999, *ApJ*, 520, 621
- Blandford, R.D. 2008, in *ASP Conf. Ser.*, 386, ed. T.A. Rector & D.S. De Young, 1
- Blandford, R.D., & Königl, A. 1979, *ApJ*, 232, 34
- Blandford, R.D., & Payne, D.G., 1982, *MNRAS*, 199, 883
- Blandford, R.D., & Znajek, R.L., 1977, *MNRAS*, 179, 433
- Bloom, S.D., & Marscher, A.P. 1996, *ApJ*, 461, 657
- Bower, G.C., Wright, M.C.H., Falcke, H., & Backer, D.C. 2003, *ApJ*, 588, 331
- Brocksopp, C., Fender, R.P., & Pooley, G.G. 2002, *MNRAS*, 336, 699
- Broderick, A.E., Fish, V.L., Doeleman, S.S., & Loeb, A. 2009, *ApJ*, 697, 45
- Broderick, A.E., Fish, V.L., Doeleman, S.S., & Loeb, A. 2011a, *ApJ*, 735, 110
- Broderick, A.E., Fish, V.L., Doeleman, S.S., & Loeb, A. 2011b, *ApJ*, 738, 38
- Broderick, A.E., & Loeb, A. 2006, *MNRAS*, 367, 905
- Broderick, A.E., & Loeb, A. 2009, *ApJ*, 697, 1164
- Broderick, A.E., Loeb, A., & Narayan, R. 2009b, *ApJ*, 701, 1357
- Broderick, A.E., Loeb, A., & Reid, M.J. 2011c, *ApJ*, 735, 57
- Bromley, B.C., Melia, F., & Liu, S. 2001, *ApJ*, 555, L83
- Browne, I. 2012, *Mem. Soc. Astron. Ital.*, 83, 925
- Brunthaler, A., et al. 2012, *Astron. Nachr.*, 332, 461
- Buscher, D.F. 1994, *IAU Symp.* 158, 91
- Camilo, F. 2008, *Nature Physics*, 4, 353
- Camilo, F., et al. 2007, *ApJ*, 669, 561
- Camilo, F., Reynolds, J., Johnston, S., Halpern, J.P., & Ransom, S.M. 2008, *ApJ*, 679, 681
- Caproni, A., Mosquera Cuesta, H.J., & Abraham, Z. 2004, *ApJ*, 616, L99
- Carilli, C.L., Bartel, N., & Diamond, P. 1994, *AJ*, 108, 64
- Carilli, C.L., Menten, K.M., Stocke, J.T., Perlman, E., Vermeulen, R., Briggs, F., de Bruyn, A.G., Conway, J., & Moore, C.P. 2000, *Phys. Rev. Lett.*, 85, 26
- Cawthorne, T.V. 2006, *MNRAS*, 367, 851
- Cernicharo, J., Pardo, J.R., & Weiss, A. 2006, *ApJ*, 646, L49
- Charlot, P., & Bourda, G. 2012 *Mem. Soc. Astron. Ital.*, 83, 959
- Chatterjee, R., et al. 2009, *ApJ*, 704, 1689
- Chatterjee, R., et al. 2011, *ApJ*, 734, 43
- Cheung, C.C., Harris, D.E., & Stawarz, Ł. 2007, *ApJ*, 663, L65
- Cohen, M.H., Lister, M.L., Homan, D.C., Kadler, M., Kellermann, K.I., Kovalev, Y.Y., & Vermeulen, R.C. 2007 *ApJ*, 658, 232
- Cordes, J.M., & Lazio, T.J.W. 2007, *ApJ*, 475, 557
- D'Arcangelo, F.D., et al. 2007, *ApJ*, 659, L107
- Daniel, F., & Cernicharo, J. 2013, *A&A*, 553, 70
- Danilenko, A.A., Zyuzin, D.A., Shibanov, Y.A., & Zharikov, S.V. 2011, *MNRAS*, 415, 867
- De Villiers, J. & Hawley, J.F. 2003, *ApJ*, 589, 458
- Deneva, J.S., Cordes, J.M., & Lazio, T.J.W. 2009, *ApJ*, 702, L177
- Dermer, C.D., & Schlickeiser, R. 1994, *ApJS*, 90, 945
- Desmurs, J.-F., Bujarrabal, V., Colomer, F., & Alcolea, J. 2000, *A&A*, 360, 189
- Dexter, J., Agol, E., Fragile, P.C., & McKinney, J.C. 2010, *ApJ*, 717, 1092
- Dexter, J., McKinney, J.C., & Agol, E. 2012, *MNRAS*, 421, 1517
- Dhawan, V., Mirabel, I.F., & Rodríguez, L.F. 2000, *ApJ*, 543, 373
- Di Matteo, T., Springel, V., & Hernquist, L. 2005, *Nature*, 433, 604
- Doeleman, S. et al. 2002, *Proc. 6th EVN Symp.*, 223
- Doeleman, S.S., et al. 2008, *Nature*, 455, 78
- Doeleman, S.S., et al. 2012, *Science*, 338, 355
- Doeleman, S.S., Fish, V.L., Broderick, A.E., Loeb, A., & Rogers, A.E.E. 2009, *ApJ*, 695, 59
- Doeleman, S.S., Lonsdale, C.J., Kondratko, P.T., & Predmore, C.R. 2004, *ApJ*, 607, 361
- Done, C., Wardziński, G., & Gierliński, M. 2004, *MNRAS*, 349, 393
- Eatough, R.P., et al. 2013, *Nature*, in press, arXiv:1308.3147
- Eckart, A., et al. 2006, *A&A*, 450, 535
- Edwards, P.G., Giovannini, G., Cotton, W.D., Feretti, L., Fujisawa, K., Hirabayashi, H., Lara, L., & Venturi, T. 2000, *PASJ*, 52, 1015
- Esin, A.A., Narayan, R., Cui, W., Grove, J.E., & Zhang, S.-N. 1998, *ApJ*, 505, 854
- Falcke, H., Mannheim, K., & Biermann, P.L. 1993, *A&A*, 278, L1
- Falcke, H., & Markoff, S.B. 2013, *Classical & Quantum Gravity*, submitted
- Falcke, H., Melia, F., & Agol, E. 2000, *ApJ*, 528, L13
- Faucher-Giguère, C.-A., & Loeb, A. 2011, *MNRAS*, 415, 3951
- Fender, R.P., Pooley, G.G., Durouchoux, P., Tilanus, R.P.J., & Brocksopp, P. 2000, *MNRAS*, 312, 853
- Fender, R.P., Garrington, S.T., McKay, D.J., Muxlow, T.W.B., Pooley, G.G., Spencer, R.E., Stirling, A.M., & Waltman, E.B. 1999, *MNRAS*, 304, 865
- Fish, V.L., Doeleman, S.S., Broderick, A.E., Loeb, A., & Rogers, A.E.E. 2009, *ApJ*, 706, 1353
- Fish, V.L., et al. 2011, *ApJ*, 727, L36
- Fujii, T., Deguchi, S., Ita, Y., Izumiura, H., Kameya, O., Miyazaki, A., & Nakada, Y. 2006, *PASJ*, 58, 529
- Gabuzda, D.C., Murray, É., & Cronin, P. 2004, *MNRAS*, 351, L89
- Gebhardt, K., Adams, J., Richstone, D., Lauer, T.R., Faber, S.M., Gültekin, K., Murphy, J., & Tremaine, S. 2011, *ApJ*, 729, 119
- Genzel, R., Schödel, R., Ott, T., Eckart, A., Alexander, T., Lacombe, F., Rouan, D., & Aschenbach, B. 2003, *Nature*, 425, 934
- Ghez, A.M., et al. 2008, *ApJ*, 689, 1044
- Gillessen, S., Eisenhauer, F., Fritz, T.K., Bartko, H., Dodds-Eden, K., Pfuhl, O., Ott, T., & Genzel, R. 2009b, *ApJ*, 707, L114
- Gillessen, S., Eisenhauer, F., Trippe, S., Alexander, T., Genzel, R., Martins, F., & Ott, T. 2009a, *ApJ*, 692, 1075
- Giroletti, M., Giovannini, G., Cotton, W.D., Taylor, G.B., Pérez-Torres M.A., Chiaberge, M., & Edwards, P.G. 2008, *A&A*, 488, 905
- Glampedakis, K., & Babak, S. 2006, *Classical & Quantum Gravity*, 23, 4167
- Goddi, C., Greenhill, L.J., Chandler, C.J., Humphreys, E.M.L., Matthews, L.D., & Grey M.D. 2009, *ApJ*, 698, 1165
- Gómez, J.L., Marscher, A.P., Jorstad, S.G., Agudo, I., & Roca-Sogorb, M. 2008, *ApJ*, 681, L69
- Gómez, J.L., Martí, J.M., Marscher, A.P., Ibáñez, J.M., & Alberdi, A. 1997, *ApJ*, 482, L33
- Gómez, J.L., Martí, J.M., Marscher, A.P., Ibáñez, J.M., & Marcaide, J.M. 1995, *ApJ*, 449, L19
- Gómez, J.L., Roca-Sogorb, M., Agudo, I., Marscher, A.P., & Jorstad, S.G. 2011, *ApJ*, 733, 11
- Gray, M.D., Wittkowski, M., Scholz, M., Humphreys, E.M.L., Ohnaka, K., & Boboltz, D. 2009, *MNRAS*, 394, 51
- Hada, K., Akihiro, D., Motoki, K., Hiroshi, N., Yoshiaki, H., & Kawaguchi, N. 2011, *Nature*, 477, 185
- Hada, K., et al. 2012, *ApJ*, 760, 52
- Hada, K., et al. 2013, *ApJ*, 775, 70
- Hagiwara, Y. 2007, *AJ*, 133, 1176
- Hawley, S.A., & Krolik, J.H. 2006, *ApJ*, 641, 103
- Henkel, C., et al. 2009, *A&A*, 500, 725
- Henri, G., & Saugé, L. 2006, *ApJ*, 640, 185
- Herrnstein, J.R., et al. 1999, *Nature*, 400, 539
- Hirota, T., Kim, M.K., & Honma, M. 2012, *ApJ*, 757, L1
- Hjellming, R.M., & Johnston, K.J. 1988, *ApJ*, 328, 600
- Homan, D.C., Lister, M.L., Aller, H.D., Aller, M.F., & Wardle, J.F.C. 2009, *ApJ*, 696, 328
- Honma, M., et al. 2012, *PASJ*, 64, 136
- Hovatta, T., Lister, M.L., Aller, M.F., Aller, H.D., Homan, D.C., Kovalev, Y.Y., Pushkarev, A.B., & Savolainen, T. 2012, *AJ*, 144, 105
- Humphreys, E.M.L. 2005, Greenhill, L.J., Reid, M.J., Beuther, H., Moran, J.M., Gurwell, M., Wilner, D.J., & Kondratko, P.T. 2005, *ApJ*, 634, L133
- Humphreys, E.M.L. 2007, *IAU Symp.* 242, 471
- Inoue, K.T., & Chiba, M. 2005, *ApJ*, 633, 23
- Ireland, M.J., Monnier, J.D., & Thureau, N. 2006, *Proc. SPIE*, 6268, 62681T
- Izumiura, H., Ukita, N., & Tsuji, T. 1995, *ApJ*, 440, 728

- Jin, C., Garrett, M.A., Nair, S., Porcase, R.W., Patnaik, A.R., & Nan, R. 2003, *MNRAS*, 340, 1309
- Johannsen, T., et al. 2012, *ApJ*, 758, 30
- Johannsen, T., & Psaltis, D. 2010a, *ApJ*, 716, 187
- Johannsen, T., & Psaltis, D. 2010b, *ApJ*, 718, 446
- Johnston, S., Kramer, M., Lorimer, D.R., Lyne, A.G., McLaughlin, M., Klein, B., & Manchester, R.N. 2006, *MNRAS*, 373, L6
- Jordan, C.H., Walsh, A.J., Lowe, V., Lo, N., Purcell, C.R., Voronkov, M.A., & Longmore, S. 2013, *MNRAS*, 429, 469
- Jorstad, S.G., et al. 2010, *ApJ*, 715, 362
- Junor, W., Biretta, J.A., & Livio, M. 1999, *Nature*, 401, 891
- Katz, J.I. 1997, *ApJ*, 478, 527
- Kellermann, K.I., et al. 2004, *ApJ*, 609, 539
- Komossa, S. 2006, *Mem. Soc. Astron. Ital.*, 77, 733
- Komossa, S., Burwitz, V., Hasinger, F., Predehl, P., Kaastra, J.S., & Ikebe, Y. 2003, *ApJ*, 582, L15
- Königl, A. 1981, *ApJ*, 243, 700
- Kovalev, Y.Y., Lister, M.L., Homan, D.C., & Kellermann, K.I. 2007, *ApJ*, 668, L27
- Kramer, M. 1995, Ph.D. thesis, University of Bonn
- Kramer, M., Klein, B., Lorimer, D.R., Müller, P., Jessner, A., & Wielebinski, R. 2000, *ASP Conf. Ser.* 202, 37
- Kramer, M., Stappers, B.W., Jessner, A., Lyne, A.G., & Jordan, C.A. 2007, *MNRAS*, 377, 107
- Kramer, M., Xilouris, K.M., Jessner, A., Wielebinski, R., & Timofeev, M. 1996, *A&A*, 306, 867
- Krichbaum, T.P., Alef, W., Witzel, A., Zensus, J.A., Booth, R.S., Greve, A., & Rogers, A.E.E. 1998, *A&A*, 329, 873
- Krichbaum, T.P., et al. 2008, *Proc. 9th EVN Symp.*, arXiv:0812.4211
- Krichbaum, T.P., Lee, S.S., Lobanov, A.P., Marscher, A.P., & Gurwell, M.A. 2008, *ASP Conf. Ser.*, 386, 186
- Kudryavtseva, N.A. 2008, Ph.D. thesis, U. Cologne
- Kudryavtseva, N.A., et al. 2011, *A&A*, 526, A51
- Kuo, C.Y., et al. 2011, *ApJ*, 727, 20
- Laing, R.A., & Bridle, A.H. 2002, *MNRAS*, 336, 328
- Levy, G.S., et al. 1986, *Science*, 234, 187
- Linfield, R.P., et al. 1989, *ApJ*, 336, 1105
- Linfield, R.P., et al. 1990, *ApJ*, 358, 350
- Liu, K., Wex, N., Kramer, M., Cordes, J.M., & Lazio, T.J.W. 2012, *ApJ*, 747, 1
- Lo, K.Y. 2005, *ARA&A*, 43, 625
- Lobanov, A.P. 1998, *A&A*, 330, 79
- Löhmer, O., Jessner, A., Kramer, M., Wielebinski, R., & Maron, O. 2008, *A&A*, 480, 623
- Lorimer, D.R., & Kramer, M. 2005, *Handbook of Pulsar Astronomy*, Cambridge U. Press (Cambridge)
- Lovelace, R.V.E., Berk, H.L., & Contopoulos, J. 1991, *ApJ*, 379, 696
- Ly, C., Walker, R.C., & Junor, W. 2007, *ApJ*, 660, 200
- Lyne, A.G., & Smith, F.G. 2005, *Pulsar Astronomy*, 3rd ed., Cambridge U. Press (Cambridge)
- Macquart, J.-P., Kanekar, N., Frail, D., & Ransom, S.M. 2010, *ApJ*, 715, 939
- Malbet, F. et al., 2010, *Proc. SPIE 7734*, 77342N
- Mannheim, K., Biermann, P.L., & Kruells, W.M. 1991, *A&A*, 251, 723
- Maoz, E. 1998, *ApJ*, 494, L181
- Markoff, S., Bower, G.C., & Falcke, H. 2007, *MNRAS*, 379, 1519
- Marrone, D.P., et al. 2008, *ApJ*, 682, 373
- Marscher, A.P. 1983, *ApJ*, 264, 296
- Marscher, A.P., et al. 2008, *Nature*, 452, 966
- Marscher, A.P., et al. 2010, *ApJ*, 710, L126
- Martí-Vidal, I., et al. 2012, *A&A*, 542, A107
- Martí-Vidal, I., et al., 2013, *A&A*, in press, arXiv:1309.0638
- Matthews, L.D., Greenhill, L.J., Goddi, C., Chandler, C.J., Humphreys, E.M.L., & Kunz, M.W. 2010, *ApJ*, 708, 80
- McKinney, J.C., & Narayan, R. 2007, *MNRAS*, 375, 513
- McKinney, J.C., Tchekhovskoy, A., & Blandford, R.D. 2012, *MNRAS*, 423, 3083
- McNamara, B.R., Nulsen, P.E.J., Wise, M.W., Rafferty, D.A., Carilli, C., Sarazin, C.L., & Blanton, E.L. 2005, *Nature*, 433, 45
- Meier, D.L., Koide, S., & Uchida, Y. 2001, *Science*, 291, 84
- Menten, K.M., Reid, M.J., Eckart, A., & Genzel, R. 1997, *ApJ*, 475, L111
- Michel, F.C. 1982, *Rev. Mod. Phys.*, 54, 1
- Michel, F.C. 1991, *Theory of Neutron Star Magnetospheres*, U. Chicago Press (Chicago)
- Mignard, F. 2012, *Mem. Soc. Astron. Ital.*, 83, 918
- Müller, J.M., Pooley, G.G., Fabian, A.C., Nowak, M.A., Reis, R.C., Cackett, E.M., Pottschmidt, K., & Wilms, J. 2012, *ApJ*, 757, 11
- Mimica, P., Aloy, M.-A., Agudo, I., Martí, J.M., Gómez, J.L., & Miralles, J.A. 2009, *ApJ*, 696, 1142
- Mirabel, I.F., & Rodríguez, L.F. 1994, *Nature*, 371, 46
- Miyoshi, M., Moran, J., Herrnstein, J., Greenhill, L., Nakai, N., Diamond, P., & Inoue, M. 1995, *Nature*, 373, 127
- Morris, D., et al. 1997, *A&A*, 322, L17
- Moór, A., Frey, S., Lambert, S.B., Titov, O.A., & Bakos, J. 2011, *AJ*, 141, 178
- Mościbrodzka, M., Gammie, C.F., Dolence, J.C., Shiokawa, H., & Leung, P.K. 2009, *ApJ*, 706, 497
- Muller, S., & Guélin, M. 2008, *A&A*, 491, 739
- Muller, S., Guélin, M., Dumke, M., Lucas, R., & Combes, F. 2006, *A&A*, 458, 417
- Muller, S., et al. 2011, *A&A*, 535, A103
- Muller, S., et al. 2013, *A&A*, 551, A109
- Mutel, R.L., & Denn, G.R. 2005, *ApJ*, 623, 79
- Nakamura, M., & Meier, D.L. 2004, *ApJ*, 617, 123
- Narayan, R. 1996, *ApJ*, 462, 136
- Narayan, R., Yi, I., & Mahadevan, R. 1995, *Nature*, 374, 623
- Neufeld, D.A., & Melnick, G.J. 1991, *ApJ*, 368, 215
- Nishikawa, K., Richardson, G., Koide, S., Shibata, K., Kudoh, T., Hardee, P., & Fishman, G.J. 2005, *ApJ*, 625, 60
- Orosz, J.A., McClintock, J.E., Aufdenberg, J.P., Remillard, R.A., Reid, M.J., Narayan, R., & Gou, L. 2011, *ApJ*, 742, 84
- O'Sullivan, S.P., & Gabudza, D.C. 2009, *MNRAS*, 400, 26
- O'Sullivan, S.P., Gabudza, D.C., & Gurvits, L.I. 2011, *MNRAS*, 415, 3049
- Owen, F.N., O'Dea, C.P., Inoue, M., & Eilek, J.A. 1985, *ApJ*, 294, L85
- Paragi, Z., Vermeulen, R.C., Fejes, I., Schilizzi, R.T., Spencer, R.E., & Stirling, A.M. 1999, *A&A*, 348, 910
- Pérez-Sánchez, A.F., & Vlemmings, W. 2013, *A&A*, 551, A15
- Pooley, G.G., Fender, R.P., & Brocksopp, C. 1999, *MNRAS*, 302, L1 ]
- Popović, L.Č., et al. 2012, *A&A*, 538, A107
- Qian, S.-J., et al. 2007, *ChJAA*, 7, 364
- Reid, M.J. 2009a, *Intl. J. Mod. Phys. D*, 18, 88
- Reid, M.J., Braatz, J.A., Condon, J.J., Greenhill, L.J., Henkel, C., & Lo, K.Y. 2009b, *ApJ*, 695, 287
- Reid, M.J., Braatz, J.A., Condon, J.J., Lo, K.Y., Kuo, C.Y., Impellizzeri, C.M.V., & Henkel, C. 2013, *ApJ*, 767, 154
- Reid, M.J., Broderick, A.E., Loeb, A., Honma, M., & Brunthaler, A. 2008, *ApJ*, 682, 1041
- Reid, M.J., & Brunthaler, A. 2004, *ApJ*, 616, 872
- Reid, M.J., McClintock, J.E., Narayan, R., Gou, L., Remillard, R.A., & Orosz, J.A. 2011, *ApJ*, 742, 83
- Richter, L.L., Kemball, A.J., & Jonas, J.L. 2012, *IAU Symp.* 287, 81
- Rodriguez, C., Taylor, G.B., Zavala, R.T., Peck, A.B., Pollack, L.K. & Romani, R.W. 2006, *ApJ*, 646, 49
- Ruprecht, J. 2012, *Testing General Relativity Using Millimeter Wavelength Radio Interferometry of Sgr A\**, MIT senior thesis
- Rushton, A., et al. 2012, *MNRAS*, 419, 3194
- Sato, M., Reid, M.J., Menten, K.M., & Carilli, C.L. 2013, *ApJ*, 764, 132
- Savolainen, T., Wilk, K., Valtaoja, E., & Tornikoski, M. 2008, *ASP Conf. Ser.*, 386, 451
- Sikora, M., Stawarz, Ł., Moderski, R., Nalewajko, K., & Madejski, G.M. 2009, *ApJ*, 704, 38
- Sillanpää, A., Haarala, S., Valtonen, M.J., Sundelius, B., & Byrd, G.G. 1988, *ApJ*, 325, 628
- Soria-Ruiz, R., Alcolea, J., Colomer, F., Bujarrabal, V., & Desmurs, J.-F. 2007, *A&A*, 468, L1
- Soria-Ruiz, R., Alcolea, J., Colomer, F., Bujarrabal, V., Desmurs, J.-F., Marvel, K.B., & Diamond, P.J. 2004, *A&A*, 426, 131
- Springel, V., Di Matteo, T., & Hernquist, L. 2005, *MNRAS*, 361, 776
- Stirling, A.M., Spencer, R.E., de la Force, C.J., Garrett, M.A., Fender, R.P., & Ogle, R.N. 2001, *MNRAS*, 327, 1273
- Stirling, A.M. et al. 2003, *MNRAS*, 341, 405
- Surcis, G., Tarchi, A., Henkel, C., Ott, J., Lovell, J., & Castangia, P. 2009, *A&A*, 502, 529
- Swinbank, A.M., et al. 2010, *Nature*, 464, 733
- Takahashi, R. 2004, *ApJ*, 611, 996
- Tarchi, A. 2012, *IAU Symp.* 287, 323
- Tarchi, A., Castangia, P., Henkel, C., Surcis, G., & Menten, K.M. 2011, *A&A*, 525, A91
- Tarchi, A., Henkel, C., Peck, A.B., & Menten, K.M. 2002, *A&A*, 389, L39
- Tateyama, C.E., & Kingham, K.A. 2004, *ApJ*, 608, 149
- Tchekhovskoy, A., Narayan, R., & McKinney, J.C. 2011, *MNRAS*, 418, L79
- Tigelaar, S.P., Fender, R.P., Tilanus, R.P.J., Gallo, E., & Pooley, G.G. 2004, *MNRAS*, 352, 1015
- Titov, O., Lambert, S.B., & Gontier, A.-M. 2011, *A&A*, 529, A91
- Ulvestad, J.S. 1999, *New Astron. Rev.*, 43, 531
- Ulvestad, J.S. 2000, *Adv. Sp. Res.*, 26, 735
- Uzan, J.-P. 2011, *Living Rev. Relativity*, 14, 2
- Valtaoja, E., & Teräsanta, H. 1995, *A&A*, 297, L13
- van Loon, J.T., Zijlstra, A.A., Bujarrabal, V., & Nyman, L.-Å. 2001, *A&A*, 368, 950
- Villforth, C., et al. 2010, *MNRAS*, 402, 2087

- Vlemmings, W.H.T., Humphreys, E.M.L., & Franco-Hernández, R. 2011, ApJ, 728, 149
- Walker, R.C., Ly, C., Junor, W., & Hardee, P. 2009, ASP Conf. Ser., 402, 227
- Wex, N., & Kopeikin, S. 1999, ApJ, 513, 388
- Wharton, R.S., Chatterjee, S., Cordes, J.M., Deneva, J.S., & Lazio, T.J.W. 2012, ApJ, 753, 108
- Wiklind, T., & Combes, F. 1996, Nature, 379, 139
- Wittkowski, M., et al. 2011, ASP Conf. Ser., 445, 107
- Xilouris, K.M., Kramer, M., Jessner, A., & Wielebinski, R. 1994, A&A, 288, L17
- Yuan, F., Quataert, E., & Narayan, R. 2003, ApJ, 598, 301
- Yusef-Zadeh, F., et al. 2006, ApJ, 644, 198
- Zackrisson, E., & Riehm, T. 2010, Adv. Astron., 478910
- Zackrisson, E., et al. 2013, MNRAS, 431, 2172